136-20

UCRL-CR-128099
PREPRINT

Upconversion-Pumped Luminescence Efficiency of Rare-Earth-Doped Hosts Sensitized with Trivalent Ytterbium

R. H. Page
K. I. Schaffers
P. A. Waide
J. B. Tassano
S. A. Payne
W. F. Krupke

July 26, 1997

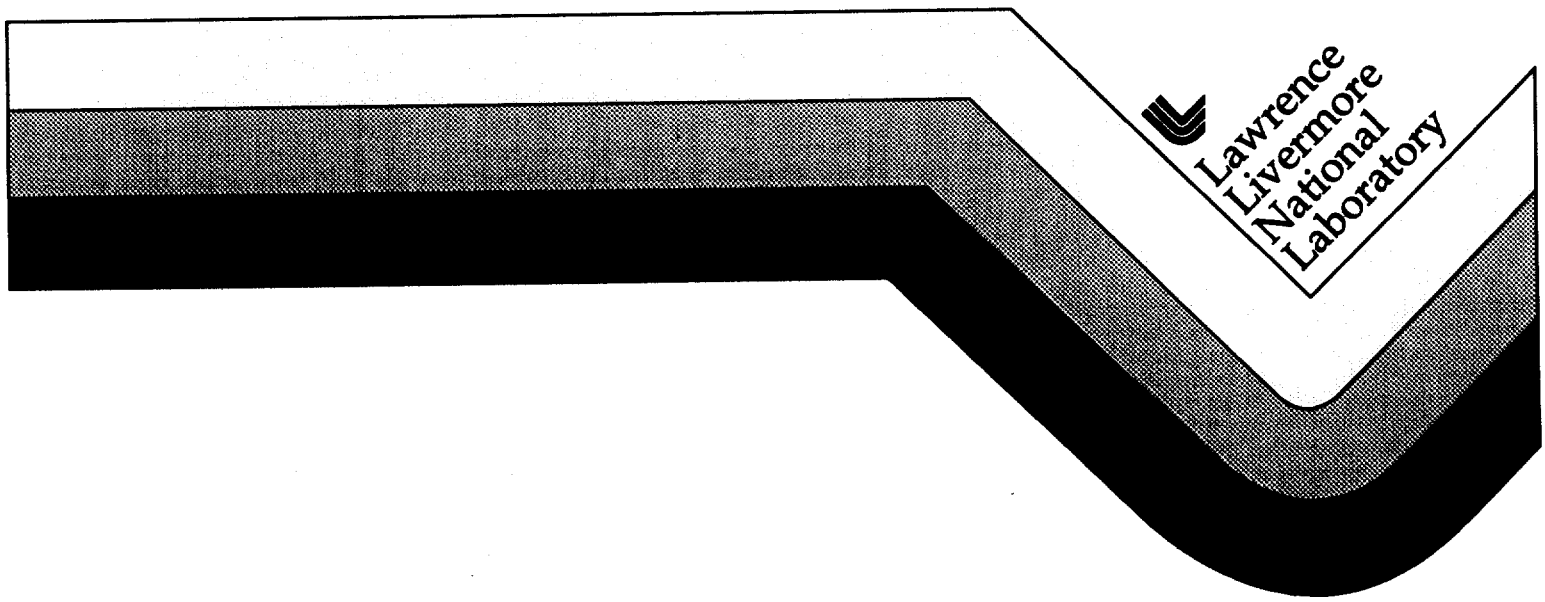

Work performed under the auspices of the U.S. Department of Energy by Lawrence Livermore National Laboratory under Contract W-7405-ENG-48.

Upconversion - Pumped Luminescence Efficiency of Rare - Earth - Doped Hosts Sensitized with Trivalent Ytterbium

Ralph H. Page, Kathleen I. Schaffers, Phillip A. Waide,
John B. Tassano, Stephen A. Payne, and William F. Krupke
Lawrence Livermore National Laboratory
University of California
Livermore, California 94550

William K. Bischel
Gemfire Corporation
2440 Embarcadero Way
Palo Alto, California 94303

Abstract

We discuss the upconversion luminescence efficiencies of phosphors that generate red, green, and blue light. The phosphors studied are single crystals and powders co-doped with Er^{3+} and Yb^{3+}, and with Tm^{3+} and Yb^{3+}. The Yb ions are pumped near 980 nm; transfers of two or three quanta to the co-doped rare earth ion generate visible luminescence. The main contribution embodied in this work is the quantitative measurement of this upconversion efficiency, based on the use of a calibrated integrating sphere, determination of the fraction of pump light absorbed, and careful control of the pump laser beam profile. The green phosphors are the most efficient, yielding efficiency values as high as 4 %, with the red and blue materials giving 1 - 2 %. Saturation was observed in all cases, suggesting that populations of upconversion steps of the ions are maximized at higher power. Quasi-CW modeling of the intensity-dependent upconversion efficiency was attempted; input data included level lifetimes, transition cross sections, and cross-relaxation rate coefficients. The saturation of the Yb,Er:fluoride media is explained as the pumping of Er^{3+} ions into a bottleneck (long-lived state)— the $^4I_{13/2}$ metastable level, making them unavailable for further excitation transfer.

1. Introduction

The promise of rare-earth-doped materials offering efficient conversion of infrared (IR) light into the visible region has long been of interest to researchers, as first discussed by Bloembergen in the context of the so-called "infrared quantum counter" [1]. The potential applications of these type of materials are many-fold, however, ranging from simple hand-held devices used to find infrared laser beams [2], to visible laser sources [3], incoherent sources [4], enhanced detection of IR light [1], and display technologies [4]. With the compelling and diverse range of applications based on these materials, we were surprised to recognize the paucity of data focused on direct and unambiguous measurements of the efficiency of the upconversion process — wherein both the emission efficiency, as well as the absorbed pump light and intensity are both quantitatively

assessed. We have pursued such a campaign, although its scope has been limited to materials co-doped with either ytterbium-erbium or ytterbium-thulium. Depending on the host medium, these two combinations can offer red, green, and blue (RGB) emission, based on infrared excitation at about 980 nm. The basic concept underlying these types of phosphors is that of initially exciting the Yb^{3+} ions, followed by multiple transfers of the energy (of ~10,000 cm^{-1}) to the visible-emitting Er^{3+} or Tm^{3+} ions.

The main accomplishment contained in this paper is the acquisition of quantitative efficiency data; the basic upconversion processes have long been known and recognized [5]. In particular, the pioneering work of Auzel led to the recognition that RGB upconversion capability is inherent among the co-doped media noted above [5]. To execute the efficiency measurements we have relied on three experimental procedures: (1) homogenizing the pump beam profile in a multi-mode fiber, (2) employing a calibrated integrating sphere to measure the visible output power, and (3) determining the fraction of absorbed pump light. Availability of a powerful, tunable laser for the phosphor excitation is a salient advantage with respect to the early work on this subject. It is noteworthy that the efficiencies (defined as emitted power in a desired color divided by power absorbed by the phosphor) reached at least 1 % in the red, 4 % in the green, and 2 % in the blue for various phosphors. All phosphors revealed a significant degree of saturation in the pump- intensity range of 10 - 1000 Watts/cm^2. Finally, we present some thoughts and a model concerning the mechanisms of efficiency saturation.

2. Phosphor samples

The upconversion phosphors tested in the present study were obtained from two sources as noted in Table 1: powders from Sarnoff Research Laboratories in Princeton, New Jersey; and single crystals grown at Lawrence Livermore National Laboratory (LLNL). Phosphor powders from Sarnoff Laboratories included two samples of $NaYF_4$:Yb,Er, Y_2O_2S:Yb,Er, Y_2O_3:Yb,Er, and Y_2O_2S:Yb,Tm. The compositional purity of each of these powders was determined by using powder x-ray diffraction utilizing Cu Kα radiation. The fluoride powders were found to be multi-phase. One of the $NaYF_4$:Yb,Er powders was synthesized using a technique that involves Na_2SiF_6 as a starting component, and SiF_4 is liberated as a by-product. X-ray diffraction indicated percentages of $Na_2Y_3F_{11}$, Na_2SiF_6, YF_3, ErF_3, and NaF to be present as impurities. In fact, the major components in this sample were YF_3 and Na_2SiF_6 which likely result from incomplete reaction of the starting reagents [6]. A second $NaYF_4$:Yb,Er sample, synthesized by an alternative method, only showed YOF as an impurity phase. X-ray diffraction analysis of the yttrium oxysulfides and the yttrium oxide indicated single-phase powders.

The LLNL $Na_2Y_3F_{11}$:Yb,Er and $Na_2Y_3F_{11}$:Yb,Tm samples were made by slowly cooling a stoichiometric melt from approximately 1000°C to room temperature over a period of 74 hours. The purities of the starting materials were 99.99% or greater. Under these circumstances it was possible to harvest crystals 3-10 mm^3. The ease with which $Na_2Y_3F_{11}$ can be grown as a single crystal has been well documented in the literature [7]. Although the results we report here are for the composition shown in Table 1, a series of crystals have been grown in which the Er andYb concentrations were independently varied. The green output was highest for the composition discussed. The red:green ratio also

depended on the composition, with red being emphasized at higher Yb doping levels. The optimal concentrations of Yb and Er for producing green upconversion appeared to be 18.0 and 2.0 mol%, respectively.

Most of the phosphors obtained from Sarnoff have been previously reported in the literature, including $NaYF_4$:Yb,Er [6,8], Y_2O_2S:Yb,Er [9], Y_2O_3:Yb,Er [10], and Y_2O_2S:Yb,Tm [9]. These materials are only available as powders, and cannot be readily grown as single crystals (in contrast to the $Na_2Y_3F_{11}$ material). A significant number of other Yb/rare-earth co-doped phosphors have been discussed and evaluated, including green emitters — YF_3:Yb,Er [11,12,13,14], BaY_2F_8:Yb,Er [11], $LiYF_4$:Yb,Er [11], $BaYF_5$:Yb,Er [13,15], and LaF_3:Yb,Er [16,17], as well as fluoride glasses [18] and oxy-fluoride ceramics [19]; red emitters — YOCl:Yb,Er [12,13] and $BaYF_5$:Yb,Er [15]; and blue emitters — YF_3:Yb,Tm [12,13,14,20] and $BaYF_5$:Yb,Tm [15]. Chloride hosts have also been examined [21].

Table 1: Powder and crystalline phosphor samples studied in the present work.

Sample Composition	Morphology	Source	% Absorbed	Emitter
$NaYF_4$:Yb,Er	powder	Sarnoff	27	green
$Na_2Y_{2.8}Yb_{0.18}Er_{0.02}F_{11}$	single crystal	LLNL	24	green
Y_2O_2S:Yb,Er	powder	Sarnoff	31	green
Y_2O_3:Yb,Er #1	powder	Sarnoff	40	red
Y_2O_3:Yb,Er #2	powder	Sarnoff	28	red
$NaYF_4$:Yb,Tm	powder	Sarnoff	54	blue
$Na_2Y_{2.64}Yb_{0.35}Tm_{0.001}F_{11}$	single crystal	LLNL	37	blue
Y_2O_2S:Yb,Tm	powder	Sarnoff	24	blue

3. Apparatus

The setup used to acquire the luminescence efficiency data (namely, pump intensity, absorbed pump power, and emitted visible power) for the phosphors is pictured in Figure 1(a). A tunable, continuous-wave Ar^+-pumped Ti:sapphire laser of up to ~1 Watt power was chopped to a 50% duty factor at 100 Hz to facilitate synchronous detection of the signal. The near-diffraction-limited beam was focused into a multi-mode fiber having a core of 200, 600, or 1000 μm diameter, in order to homogenize the beam and format its intensity profile into a "top-hat." To minimize uncertainty in the exciting beam diameter, the fiber was simply butted up against the sample holder, which was located at the rear of an integrating sphere. Use of fibers of different diameters provided crude control of the pump intensity, and a series of calibrated ND filters gave fine adjustment in small, discrete steps. The fiber jackets were stripped to avoid introducing lossy elements into the integrating sphere. A graded ND wheel upstream of the fiber coupler allowed setting of the maximum power launched into the fiber. Red luminescence from the Ti:sapphire rod was blocked with a Hoya IR-83 (long-pass) filter.

The sample holder [Figure 1(b)] was constructed by placing a 12 mm square, 500 μm thick stainless steel spacer between two microscope slide cover slips, and including a 3 mm diameter opening for the powder sample to reside with a 1 mm wide access port. This arrangement kept the luminescent zone ~1 mm away from the stainless steel parts, whose reflectivity is below that of Spectralon, the construction material of the integrating sphere. Single-crystal samples could be mounted in lieu of the powder holder, also at the rear of the integrating sphere. Powder samples appeared sensibly opaque to the eye, and positioning the samples so that their "front" (pumped) sides faced the inside of the integrating sphere gave larger signals than the alternative arrangement. Upon being filled with phosphor powder, the sample holders were shaken slightly to compact the powder.

Dichroic color - separation filters, doped-glass color filters, and a Spectralon aperture were used at the interface between the integrating sphere and the ET-4000 (silicon) photodiode. A lock-in amplifier recorded the magnitude of the signal delivered to its "virtual ground" input via a coaxial cable. The wavelength-dependent integrating-sphere/photodiode response (affected by the color filters, the sample holder, etc.) was calibrated by introducing known power levels of helium-neon (543 and 633 nm) and Kr-ion (479, 520, 568, and 647 nm) laser light into the sphere. The sample-holder parts, some of which were metal, noticeably degraded the integrating sphere's responsivity, and there was a significant wavelength dependence to the overall sensitivity, so the responsivity characterization was quite important. Typical responsivity values for our setup were in the range 25 - 50 Volt / Watt, and with the lock-in amplifier, detection of powers as low as 1 μW was feasible.

In the case of single-crystal samples, absorption spectra were simple to obtain, and the "fraction absorbed" FA of the pump light was calculated with the expression

$$FA = 1 - 10^{-OD},$$

where OD is the optical density of the crystal at the pump wavelength, as measured with a spectrophotometer. The Yb^{3+} peak absorption coefficient α_{975} [cm^{-1}] in the $Na_2Y_{3-z-x}F_{11}:Yb_z,Er_x$ varied roughly as $\alpha_{975} \sim 30z$.

The fraction of Ti:sapphire pump light absorbed by a powder sample was much more difficult to assess. It was determined with recourse to the identity

$$R + T + FA = 1,$$

where R represents the sample's (diffuse) reflectance, T is its transmittance, and FA is the "fraction absorbed" of pump light. Measurements of FA have been reported with use of a spectrophotometer's diffuse-reflectance attachment [14], but we used the chopped, tunable Ti:Sapphire laser running at a low light level, and lock-in detection with the integrating sphere. To measure transmittance (T) values, we placed the powder samples at the "mouth" of the integrating sphere, so as to detect light that passed all the way through the sample. For obtaining reflectance values, the samples were placed in their customary position at the

"far" end of the sphere. Since the light absorbed by Yb^{3+} can be re-radiated at nearly the same wavelength as the pump, we were faced with the problem of discriminating against fluorescence. This was accomplished by using a chopping frequency high with respect to the radiation rate, peaking the phase - sensitive detector carefully, and using a 975 nm interference filter to reject the (mostly-longer-wavelength) fluorescence.

To calibrate the responsivity of the integrating sphere / sample holder / photodiode combination in order to obtain a baseline (FA = 0) point, we tuned the probe laser to an off - resonance wavelength (1040 nm) as well as the ~975 nm wavelength used to excite upconversion luminescence. Also, we measured powder-sample properties relative to the "reflection - mode" signal from a white, non-absorbing (Spectralon) "reference standard" plug. With primes denoting signal ratios with respect to the reference standard and subscripts denoting the probe wavelength, we obtained values for R'_{975}, T'_{975}, R'_{1040}, and T'_{1040}. Because of the sensitivity reduction caused by sample-holder parts, these values are uniformly reduced by a common factor S with respect to the actual sample values. With a little arithmetic [and since $(R_{1040} + T_{1040}) = 1$] it is possible to normalize out the sensitivity ratio S:

$$FA = 1 - (R'_{975} + T'_{975}) / (R'_{1040} + T'_{1040}) \qquad (1)$$

The luminescence spectra were recorded by simply collecting the emission from the sample and employing a spectrograph equipped with a photodiode array and an optical multi-channel analyzer (EG&G PAR Corporation). The diode array was calibrated using a blackbody source.

Lastly, emission lifetime data were obtained using a frequency-doubled, Q-switched Nd:YAG laser / pulsed dye laser system, detecting the wavelength - resolved emission with a photomultiplier tube, and storing the data with a transient digitizer. Raman-shifting the dye laser's red output gave tunable light around 980 nm for exciting the Yb^{3+} transition, and direct use of 532 nm light allowed excitation of the green-emitting Er^{3+} $^4S_{3/2}$ level.

4. Results

The emission spectra of the eight samples explored in the study are shown in Figs. 2(a), 2(b), and 2(c), for the green, red, and blue emitters, respectively. Although the "green" emitters appear to radiate significantly in the red as well, the naturally-green-peaked sensitivity of the human eye assures that in most cases, they appear mostly green. In some phosphors (e.g. our TOKIN "IR catcher" card, which is partly based on YF_3 [2, 21], and the $NaYF_4$ - based phosphor) the pump-intensity dependencies of the red and green emissions are quite different, with the red increasing much faster. A yellowish appearance is obtained at high intensity. Interestingly, even though the red and the green phosphors both contain Yb and Er co-dopants, the pure oxides provide overwhelmingly red emission. This is because the green and red emissions arise from different electronic transitions ($^4S_{3/2} \rightarrow {}^4I_{15/2}$ versus $^4F_{9/2} \rightarrow {}^4I_{15/2}$, respectively). It is the rapid $^4S_{3/2} \rightarrow$

$^4F_{9/2}$ nonradiative decay that renders the "green" level non-emissive in the pure oxides; this issue will be discussed further below. In Fig. 2C, the 480 nm band of the Yb,Tm doped media is seen to give rise to the blue color of these phosphors. It is seen that the transition energies are somewhat host-dependent and that the detailed lineshapes vary from one host to another. In general, the oxysulfides (Y_2O_2S) exhibit the sharpest emission features and have transitions at slightly longer wavelengths than the fluorides and oxides.

The efficiencies characteristic of each of the phosphor colors are depicted in Figs. 3(a), 3(b), and 3(c). Selective detection of the different upconversion signals was achieved with optical filters that isolated the desired colors. Here the efficiency corresponds to the emitted power with the desired color, divided by the *absorbed* pump light at the optimum wavelength (near 980 nm). (The FA correction has been made in the conversion-efficiency scale.) The pump intensity scale is the incident intensity on the sample surface. In cases where more than one fiber diameter was used for applying the pump light, it is seen that the different data sets agree reasonably well, validating our approach of using the geometric fiber cross-sectional area as the effective pump spot size.

The fluoride-based green phosphors turn out to be the most efficient, approaching 4 % power conversion. It is seen that the curves display a near-linear dependence of efficiency on pump intensity, as one would expect in a case where $P_{green} \propto I_{pump}^2$. Also, there is a tendency to saturate at high pump intensity. At first the higher efficiency (for a given pump intensity) attained by the $NaYF_4$ powder compared to the $Na_2Y_3F_{11}$ single crystal was surprising to us, in light of the more-transparent nature of optically-clear crystals. But because of multiple scattering of the pump light, its propagation is diffusive, and the powder experiences an internal intensity higher than that incident on the sample. This effect is also known in medical laser studies, where the artificial rise of intensity in tissue must be taken into account for nonlinear light-matter interactions [22]. Since all of the upconversion effects discussed in this paper are due to multi-photon absorption, and therefore supra-linear with respect to pump intensity, the pump light concentration should increase the measured efficiency, especially since we have corrected the efficiency for the absorbed fraction of the pump light. Below we only model the single crystal results, for which we have well-characterized values of the pump intensity. It is qualitatively satisfying to see, however, that the two fluoride hosts saturate at a similar efficiency value. Considering that the crystal structure of $Na_2Y_3F_{11}$ is a modification of the fluorite (CaF_2) structure and has cubic site symmetry, we expect that the Yb^{3+} absorption band will be weakest in this host, and will exhibit the highest saturation intensity. Clearly, it would be interesting to compare data for samples with identical morphologies.

From the green-phosphor efficiency plots, we can estimate the parameter μ in the relation $I_{green} = \mu I_{pump}^2$ for cases where there is the expected linear increase of efficiency with pump intensity. For $NaYF_4$:Yb,Er, $\mu \sim 10^{-2}$ cm^2/W, while for $Na_2Y_3F_{11}$:Yb,Er, $\mu \sim 2 \times 10^{-4}$ cm^2/W. Other authors have also reported μ values for various upconversion processes and materials. [5, 23, 24]

The red phosphor material studied was Y_2O_3 codoped with Er and Yb. The two samples obtained from Sarnoff were prepared with different rare earth concentrations. Here the efficiency attained a maximum value of about 1 %, somewhat less than the fluoride hosts of Fig. 2(a). The likely cause of this situation is competition from nonradiative decay for both the $^4S_{3/2}$ and $^4F_{9/2}$ states. As has been previously noted by several authors, however, these red phosphors benefit from the existence of an additional upconversion mechanism (compared to the green emitters), based on excited Yb promoting the Er ions from the $^4I_{13/2}$ metastable level directly to the red-emitting $^4F_{9/2}$ state.

The Yb,Tm co-doped materials also yielded reasonably high efficiencies of 2 %. This result is particularly favorable, considering that three energy-transfer steps from the Yb ions to the Tm ions are needed to create a blue photon. We expect a result of the sort $P_{blue} \propto I_{pump}^3$, and thus $\eta_{blue} \propto I_{pump}^2$. What is observed instead is a roughly linear, or even sub-linear power dependence rather than the quadratic one. This could imply that the upconversion process is saturated in at least one step. Previous workers have found that a large ratio of Yb to Tm ions is needed to achieve high upconversion efficiencies; [25 - 27] the Tm^{3+} density is ostensibly hundreds of times smaller than the Yb^{3+} concentration. So, given a reasonable energy-transfer probability, even a moderate level of excitation in the Yb^{3+} population would suffice to pump the majority of the Tm^{3+} ions to their first excited state, depleting the ground state and causing saturation.

The absolute efficiency values presented here seem to be roughly in line with those presented by Rich and Pinnow, [28] who used hemispherical 960 nm GaAs:Si photodiode upon which a thin layer of Yb,Er - codoped phosphor powder was attached. Absolute efficiency values from 0.2 - 0.6% were reported (with no "fraction absorbed" correction.) Regarding the pump intensity, the diode parameters were as follows: hemisphere diameter D = 36 mil (for a surface area $A_{diode} = \pi D^2/2 = .013$ cm^2); efficiency $\eta_{IR} = 0.017$, voltage V = 1.5 Volt, and current I = 0.3 Amp (for a power $P_{diode} = \eta_{IR}\, I\, V = 76.5$ mW.) The diode's output was claimed to be nonuniformly distributed over the 2π hemisphere solid angle, so its effective area was less than A_{diode}. We conclude that the pump intensity was $I_{pump}^{diode} \geq (P_{diode} / A_{diode}) \sim 6$ W cm^{-2}.

Temperature dependences have been noted in previous investigations of upconversion phosphor efficiencies; in general, heating degrades performance. [28] Since powders do not conduct heat well, significant temperature rises are to be expected with the high absorbed power density prevalent in this experiment. To investigate this effect, we compared signal levels with different heat loads, by masking some of the Ti:sapphire laser chopper's openings to change the duty factor from 50% to 3.3%. Two phosphors—$NaYF_4$:Yb,Er (green) and Y_2O_3:Yb,Er (red)—exhibited only a slight effect, but Y_2O_2S:Yb,Er (green) showed a signal roughly twice as large with the lower duty cycle. The efficiency plots of Figure 3(a, c) show that the oxysulfides exhibit the steepest efficiency rollovers as the pump intensity is increased; some of the efficiency falloff may be attributed to heating.

5. Discussion

Rich and Pinnow [28] had been interested in determining limiting (saturated) values for upconversion efficiencies, but were hampered by the lack of bright, resonant pump sources. They used a 0.8 W CW 1064 nm Nd:YAG laser focused to a 50 μm spot (presumably on a single phosphor grain) and measured the *relative* visible light signals as a function of pump intensity, which could be made ~10^4 times brighter than the GaAs:Si photodiode. Since this excitation wavelength was not quite resonant with the Yb^{3+} transition, a "detuning penalty" of 2 - 4 orders of magnitude existed. (The Nd:YAG laser is detuned ~10% (~1000 cm^{-1}) to the red of the Yb^{3+} peak.) The procedure for assigning the *effective resonant pump intensity* was to look at the red:green:blue ratios (which are intensity-dependent) of the Er^{3+} emissions and match them up with the ratios obtained with the GaAs:Si photodiode, for which an *absolute* efficiency calibration had been done. It was hoped that this correlation procedure would provide a correct extrapolation into the regime of higher resonant pump intensity, that would someday be available when more powerful photodiodes were developed. The results of this extrapolation were that in some cases (notably YF_3 and $BaYF_5$,) green upconversion efficiencies approaching 10% were predicted. The red upconversion efficiency for YF_3 was ~20%, and for BaY_2F_8 it exceeded 5%. For each of these three barium-yttrium-fluoride hosts, the efficiency had not begun to "roll over" at the maximum available pump intensity. So, even higher efficiencies were to be expected, in contrast with our new findings (Figure 3.)

Two difficulties in the intensity-correlation procedure had been explicitly noted by Rich and Pinnow. [28] First, the sample arrangements were somewhat different in the two experiments; self-absorption might have occurred in the layer of phosphor between the photodiode and the detector. Second, the phosphor grains did not all receive the same pump intensity in that configuration, so that the emission spectrum represented an intensity-average. But, we can also imagine another more subtle source of perturbation in the R:G:B ratios: direct excitation of Er^{3+} ion transitions by the 1064 nm light. This pumping mechanism is not included in the energy-transfer model used to explain upconversion. For example, the $^4F_{9/2} \leftarrow {}^4I_{13/2}$ transition is nearly-resonant with the Nd:YAG laser (but is quite far off resonance with the shorter-wavelength photodiode.) [29] This sort of transition would enhance the $^4F_{9/2}$ population, boosting the red output (which grows faster with intensity than the green,) making the phosphor appear to be more highly pumped than it really was. This would explain the very-high extrapolated efficiencies, and the lack of an observed saturation.

Green Phosphors: The modeling of the Yb-Er green phosphor was attempted in detail, owing to the significant amount of prior effort in this area. [5, 13, 15, 16, 30 - 32] We have built on the many ideas previously presented, but we have separated out the main aspects of the mechanism that we think are most crucial, made several approximations, and reduced the theory to a specific result that can be directly compared with experiment. The energy level diagram and denoted processes (Figure 4) should help to clarify the ensuing derivation.

The model we use applies in the quasi-steady-state regime, so that we calculate the average upconversion efficiency and ignore the transient behaviour of the various

populations and emitted light signals. Saturation is assumed to occur because Er^{3+} ions become trapped in the $^4I_{13/2}$ level, thus depleting the populations in the ground ($^4I_{15/2}$) and "one-absorbed-photon" ($^4I_{11/2}$) levels able to contribute to upconversion. Several physical mechanisms populate the $^4I_{13/2}$ level, and calculation of its population as a function of pump intensity is a major thrust of the following discussion.

The main experimental observable is the green upconversion signal. The green-emitting $^4S_{3/2}$ level is populated by upconversion and decays with a lifetime $\tau_{3/2}$. Its population has a steady-state value of

$$N^E_{3/2} = \gamma_{upc} N^E_{11/2} N^Y_{5/2} \tau_{3/2}, \qquad (2)$$

where γ_{upc} accounts for the induced $(^4I_{11/2} + {}^2F_{5/2}) \rightarrow (^4S_{3/2} + {}^2F_{7/2})$ upconversion transition, $N^E_{11/2}$ is the $^4I_{11/2}$ population of Er, $N^Y_{5/2}$ is the $^2F_{5/2}$ Yb population, and $\tau_{3/2}$ is the observed $^4S_{3/2}$ lifetime.

Secondly, we take the $^4I_{11/2}$ and $^2F_{5/2}$ states (of Er and Yb, respectively) to be in fast equilibrium:

$$(N^Y_{7/2} N^E_{11/2} / N^Y_{5/2} N^E_{15/2}) = (Z^Y_{7/2} Z^E_{11/2} / Z^Y_{5/2} Z^E_{15/2}) \exp(-\Delta E/kT) \qquad (3)$$

Here the Z's are the partition functions of the states designated by their respective super- and subscripts, and ΔE is the $Er^{3+}\ ^4I_{11/2}$ - $Yb^{3+}\ ^2F_{5/2}$ energy gap. A negative value for ΔE favors storage of electronic excitation in the Er^{3+} ions. As it happens, the energy levels are near-degenerate and the partition functions have similar magnitudes, so the right-hand-side of Eq. (3) is approximately unity. Thus we have $N^Y_{5/2}/N^Y_{7/2} = N^E_{11/2}/N^E_{15/2}$, or the intuitive result that the *ratio* of Yb and Er excited/ground state populations remains fixed.

The excited levels ($^4I_{11/2}$ and $^2F_{5/2}$) are observed to be strongly coupled and to exhibit a mutual decay lifetime τ_{eq}. In the limit of negligible bleaching of the Yb^{3+} transition, $N^Y_{7/2} \approx N_{Yb}$ (the Yb-doping concentration.) The $N^Y_{5/2}$ number density is then estimated as

$$N^Y_{5/2} = \alpha_p I_p \tau_{eq} / h\nu_p \equiv N_{Yb} I_p / I_{sat} \equiv N_{Yb} I_p'$$

(where α_p is the absorption coefficient at the pump wavelength; I_p is the pump intensity.) Here we have defined a pump saturation intensity $I_{sat} = h\nu_p / \sigma_p \tau_{eq}$ and a dimensionless pump intensity $I_p' = I_p / I_{sat}$.

Eqs. 2 and 3 can be combined (along with the simplifications described above) to yield the following expression for the volumetric emission rate of green photons:

$$N^E_{3/2} / \tau_{rad} = \gamma_{upc} \; N^E_{15/2} \, N_{Yb} \, (\tau_{3/2} / \tau_{rad}) \, (I_p')^2 , \qquad (4)$$

where τ_{rad} is the radiative lifetime of the $^4S_{3/2}$ state. As expected, the green signal is quadratic in the pump intensity as long as the Er^{3+} ground-state number density is not significantly depleted. If the majority of Er ions (whose number is conserved at the dopant density N_{Er}) are regarded as being in the either the $^4I_{13/2}$ or $^4I_{15/2}$ states, then:

$$N^E_{15/2} = N_{Er} - N^E_{13/2}. \qquad (5)$$

We now need to calculate the concentration of Er ions that are "bottlenecked" on the $^4I_{13/2}$ state (in the steady-state condition) with:

$$dN^E_{13/2}/dt = 0 = (\beta_{11/2}/\tau_{11/2}) \, N^E_{11/2} - N^E_{13/2}/\tau_{13/2} + \beta_{3/2} \, N^E_{3/2}/ \tau_{rad} + \gamma^X_{3/2} \, N^E_{3/2} \, N^E_{15/2} + \gamma^Y_{3/2} \, N^E_{3/2} \, N_{Yb} \qquad (6)$$

where the terms on the right-hand side describe, in sequence from left to right: radiative filling of the $^4I_{13/2}$ state from the $^4I_{11/2}$ level (whose lifetime is $\tau_{11/2}$; $\beta_{11/2}$ is the branching ratio); radiative draining of the $^4I_{13/2}$ state; radiative filling of the $^4I_{13/2}$ state from the $^4S_{3/2}$ level ($\beta_{3/2}$ is the branching ratio to the $^4I_{13/2}$ state, τ_{rad} is again the $^4S_{3/2}$ lifetime); cross relaxation between two Er ions (via the transition $^4S_{3/2} + {}^4I_{15/2} \rightarrow {}^4I_{9/2} + {}^4I_{13/2}$, whose rate coefficient is $\gamma^X_{3/2}$); and energy "back transfer" from Er to Yb, involving coupled $^4S_{3/2} \rightarrow {}^4I_{13/2}$ and $^2F_{5/2} \leftarrow {}^2F_{7/2}$ transitions, with rate coefficient $\gamma^Y_{3/2}$. Er^{3+} ions transferred to the $^4I_{9/2}$ level are not treated explicitly with a separate rate equation; we assume that they relax radiatively to the ground level or non-radiatively to the $^4I_{11/2}$ level. Since the populations in these levels are assumed to be governed by the Yb reservoir via the thermodynamics expressed in equation (3), this neglect is not a serious perturbation in the overall scheme.

To simplify manipulation of the multitude of constants in the various equations, it is convenient to define several more dimensionless variables:

$F_{casc} \equiv (\beta_{11/2} / \tau_{11/2}) \, \tau_{13/2}$ (radiative cascade that fills bottleneck level);

$F_{fill} \equiv (\beta_{3/2} / \tau_{rad}) \, \tau_{13/2}$ (radiation from green-emitting level into bottleneck);

$F_{cross} \equiv \gamma^X_{3/2} \, N_{Er} \, \tau_{13/2}$ (Er - Er cross - relaxation rate coefficient);

$F_{back} \equiv \gamma^Y_{3/2} \; N_{Yb} \, \tau_{13/2}$ (Er - Yb back - transfer cross - relaxation rate coefficient);

$F_{upc} \equiv \gamma_{upc} \, N_{Yb} \, \tau_{3/2}$ (upconversion rate constant for populating green emitter).

Equation (6) can then be rewritten as

$$N^E_{13/2} = F_{casc}\, N^E_{11/2} + (F_{fill} + F_{back})\, N^E_{3/2} + (F_{cross} / N_{Er})\, (N_{Er} - N^E_{13/2})\, N^E_{3/2}. \quad (6')$$

A re-collection of terms and insertion of the explicit pump-intensity dependencies gives a quadratic equation in $(N_{Er} - N^E_{13/2})$:

$$0 = -N_{Er} + \{1 + F_{casc}\, I_p' + F_{upc}(F_{fill} + F_{back})(I_p')^2\}(N_{Er} - N^E_{13/2}) + (F_{cross}F_{upc} / N_{Er})(I_p')^2\, (N_{Er} - N^E_{13/2})^2. \quad (7)$$

Expressions for the solution of (7) are not immediately illuminating; however, in the limit that $I_p' \rightarrow 0$, $N^E_{13/2} \rightarrow 0$, as expected. In the limit of large I_p', $N^E_{13/2}$ asymptotically approaches N_{Er} as $N^E_{13/2} \rightarrow N_{Er}\{1 - [F_{upc}(F_{fill} + F_{back})(I_p')^2]^{-1}\}$. In other words, most of the Er population is pumped into the $^4I_{13/2}$ bottleneck. According to the approximation of equation (5), the $^4I_{15/2}$ population scales as $N_{Er} / F_{upc}(F_{fill} + F_{back})(I_p')^2$, and its inverse-square intensity dependence is at the root of the rollover in upconversion efficiency.

Finally, the actual green efficiency (green Watt cm^{-3} emitted per IR pump Watt cm^{-3} absorbed) of the phosphor is calculated with

$$\eta_{green} = N^E_{3/2}\, \beta_{green}\, h\nu_{green} / \tau_{rad}\, \alpha_p\, I_p \quad (8)$$

where β_{green} is the branching ratio for the green $^4S_{3/2} \rightarrow {}^4I_{15/2}$ transition of energy $h\nu_{green}$, and the efficiency has been normalized to the power density of absorbed pump light at the surface of incidence. Upon substitution of previous formulae, (8) becomes

$$\eta_{green} = \gamma_{upc}\, (N_{Er} - N^E_{13/2})\, \tau_{eq}\, (I_p')\, (\tau_{3/2} / \tau_{rad})\, \beta_{green}\, (h\nu_{green} / h\nu_{pump}). \quad (9)$$

Again, it is important to emphasize that all of the mechanistic steps included in the derivation of eqs. (7 - 9) were previously discussed in the literature; our contribution is to invoke suitable approximations and assumptions to reduce the theory to a form amenable to straightforward comparison with experiment. In fact, all of the parameters except γ_{upc} were derivable from either the scientific literature or separate experimental measurements, as noted in Table 2. The fit to the data for the green-emitting crystal $Na_2Y_3F_{11}$:Yb,Er is displayed in Fig. 5. Our fitting procedure began with adjustment of γ_{upc} to match the low-intensity part of the data. Once $\tau_{3/2}$ has been fixed, γ_{upc} is the only other adjustable parameter that affects this part of the curve, so this step of the fitting is straightforward. In some sense, the data constrain the value of $\gamma_{upc} \bullet \tau_{3/2}$.

A comment regarding $\tau_{3/2}$ is in order. Because of Er cross-relaxation and Yb back-transfer, the observed lifetime of the Er^{3+} $^4S_{3/2}$ level can be a good deal shorter than in a lightly-doped crystal free of Yb. In the formalism we use, the overall lifetime is determined as

$$\tau_{3/2}^{-1} = \tau_{rad}^{-1} + \gamma^{X}_{3/2} N_{Er} + \gamma^{Y}_{3/2} N_{Yb}, \qquad (10)$$

with no explicit term for nonradiative decay via multiphonon emission to the $^4F_{9/2}$ level since this is a minor effect with respect to the other two quenching processes. In spite of our direct excitation of the $^4S_{3/2}$ level, measurement of $\tau_{3/2}$ is inherently difficult because the fluorescence decay is not single-exponential. The 400 μsec value we report is derived from the straight-line portion of the ln(intensity) - vs - time curve, but the initial part of the decay corresponds to a much shorter time scale. Ostermayer [13] has provided YF_3 data from which $\gamma^{X}_{3/2}$ and $\gamma^{Y}_{3/2}$ may be estimated; however, equation (10) does not accurately represent the Er-concentration-dependence of $\tau_{3/2}$, which appears to decline precipitously at ~5% Er doping. Rough values derived from data presented in [13] are shown in Table 2 (in parentheses) and are respectively $\gamma^{X}_{3/2} \sim 3 \times 10^{-17}$ cm^3/sec and $\gamma^{Y}_{3/2} \sim 5 \times 10^{-18}$ cm^3/sec.

When varying the values of $\gamma^{X}_{3/2}$ and $\gamma^{Y}_{3/2}$ during fitting, it is found that the former mainly affects the peak conversion efficiency, while the latter impacts the intensity at which the efficiency rollover begins (which in turn affects the peak efficiency.) While no combination of constants fits the data perfectly, the values in Table 2 (and fit of Fig. 5) represent a compromise—they are not wildly different from the "starting" values gleaned from [13] and lead to a calculated [eq. (10)] value for $\tau_{3/2}$ of 94 μsec. It is possible to move and shape the calculated efficiency rollover to match the data almost exactly by employing the values $\gamma^{X}_{3/2} = 1 \times 10^{-15}$ cm^3/sec and $\gamma^{Y}_{3/2} = 1 \times 10^{-19}$ cm^3/sec, but then eq. (10) yields $\tau_{3/2} = 16$ μsec, a value we consider unreasonably low. Considering the intensity-averaging inherent in our experiment (since the pump light is attenuated as it passes through the crystal,) the efficiency - vs - intensity peak is expected to smear. So, further effort to fine-tune the model is probably not warranted at this time.

A completely-general model would involve rate equations for all the populated energy levels, and since violet emission is observed from the Er^{3+}-doped samples, levels up to at least 25,000 cm^{-1} would be involved (i.e. more than a dozen.) A large number of energy-transfer processes (mostly with poorly-known rate coefficients) would also have to be considered, and such a model would be quite unwieldy. The model of Mita [31] includes many levels, but parameterizes all of the energy-transfer coefficients with an "energy-gap" relation that involves only two scale parameters. Sketched in Fig. 4(b) are some additional energy-transfer processes that explain red emission from the Yb,Er-doped phosphors. While some of these processes (radiationless decay) are more important in high-phonon-frequency (e.g. oxide) hosts, they still occur in green emitters at a lower level.

Because of energy transfer and the complex of kinetic processes, the saturation in upconversion efficiency is not expected to occur at the nominal sensitizer (Yb^{3+}) saturation intensity. In some sense, the Yb^{3+} ions "gang up" on the Er^{3+} ions, so saturation occurs at a lower intensity; with the values displayed below, this occurs at ~500 W cm^{-2}, over a factor of 10 below the nominal I_{sat}.

A main result of the saturation model is the Er^{3+} $^4I_{13/2}$ population $N^E_{13/2}$, as a function of pump intensity. It should be possible to assess this population by looking at the radiation emitted on the 1600 nm $^4I_{13/2} \rightarrow {}^4I_{15/2}$ transition.

Table 2: Values of mechanistic constants used to fit the efficiency data of Fig. 5.

Parameter	Value	Source
α_p, pump absorption coefficient	6 cm^{-1}	absorption spectrum
σ_p, pump absorption cross section	1.0 x 10^{-20} cm^2	derived from N_{Yb} and α_p
N_{Yb}, Yb concentration	6.0 x 10^{20} cm^{-3}	crystal melt conc'n
N_{Er}, Er concentration	6.0 x 10^{19} cm^{-3}	crystal melt conc'n
τ_{eq}, equilibrated $^2F_{5/2}$ / $^4I_{11/2}$ lifetime	2.8 msec	measured luminescence decay
$\tau_{3/2}$, $^4S_{3/2}$ lifetime	50 - 400 µsec	measured decay(s)
τ_{rad}, $^4S_{3/2}$ radiative lifetime	600 µsec	measured decay / estimate
$\tau_{11/2}$, $^4I_{11/2}$ lifetime	4 msec	estimate
$\tau_{13/2}$, $^4I_{13/2}$ lifetime	13 msec	measured decay
$\beta_{3/2}$, $^4S_{3/2} \rightarrow {}^4I_{11/2}$ branching ratio	0.3	Judd-Ofelt coefficients[b]
$\beta_{11/2}$, $^4I_{11/2} \rightarrow {}^4I_{13/2}$ branching ratio	0.2	Judd-Ofelt coefficients[b]
β_{green}, $^4S_{3/2} \rightarrow {}^4I_{15/2}$ branching ratio	0.7	Judd-Ofelt coefficients[b]
γ_{upc}, Er upconversion rate coefficient	1.0 x 10^{-17} cm^3s^{-1}	fitted to efficiency data
$\gamma^Y_{3/2}$, Er-Yb cross-relaxation rate coefficient	(5 x 10^{-18} cm^3s^{-1}) 5.0 x 10^{-18} cm^3s^{-1}	literature[a] fit (this work)
$\gamma^x_{3/2}$, Er - Er cross relaxation rate coefficient	(3 x 10^{-17} cm^3s^{-1}) 1.0 x 10^{-16} cm^3s^{-1}	literature[a] fit (this work)
$h\nu_{pump}$, pump photon energy	2.0 x 10^{-19} J	975 nm
$h\nu_{green}$, emitted green photon energy	3.3 x 10^{-19} J	550 nm

(a) Reference [13]; also provides good match to lifetime data obtained from crystals with different Yb doping.
(b) Reference [29]

Table 3: Definitions and values of derived parameters.

Symbol	Definition	Description	Value
F_{casc}	$(\beta_{11/2} / \tau_{11/2})\ \tau_{13/2}$	radiative cascade that fills bottleneck level	0.65
F_{fill}	$(\beta_{3/2} / \tau_{rad})\ \tau_{13/2}$	radiation from green-emitting level into bottleneck	6.5
F_{cross}	$\gamma^{X}_{3/2}\ N_{Er}\ \tau_{13/2}$	Er - Er cross - relaxation rate coefficient	78
F_{back}	$\gamma^{Y}_{3/2}\ N_{Yb}\ \tau_{13/2}$	Er - Yb back - transfer rate coefficient	39
F_{upc}	$\gamma_{upc}\ N_{Yb}\ \tau_{3/2}$	upconversion rate constant to populate green emitter	2.4
I_{sat}	$h\nu_p / \sigma_p \tau_{eq}$	pump saturation intensity	7.1 kW cm^{-2}

Red Phosphors: The red phosphors are not as well studied as the green luminophors, although the critical differences are recognized as: increased nonradiative decay from the $^4S_{3/2}$ and $^4F_{9/2}$ emitting levels (green and red emitting states, respectively), along with a likely enhanced reliance on the $^4I_{13/2}$ - $^4F_{9/2}$ upconversion mechanism to emit in the red. Both of these processes are noted in fig. 4(b). These extra processes assure an increase in the red versus the green luminescence, although the red luminescence is unlikely to be more efficient in these materials than the green luminescence was in the Yb,Er:fluorides discussed above.

Blue Phosphors: The upconversion mechanisms mediating the efficiencies of the RGB phosphors discussed in this article have been previously discussed in the literature [5, 12, 13, 15, 20, 31]. For the case of the Yb-Tm couple, the mechanism calls for three separate energy transfer steps. Interestingly, although this system operates with the highest-order inter-ion process, it turns out to also be the least controversial in the literature. In other words, the three steps are all fairly well specified, as depicted in Fig. 4(c). In addition, from a thermodynamic point of view, the substantial energy surplus of the Yb^{3+} $^2F_{5/2}$ level with respect to the Tm^{3+} $^3F_4$ level assures that (in the fast-energy-migration regime) most of the Yb excitation energy will be transferred to the Tm^{3+} $^3F_4$ level. In general, the saturation intensity for a two-level transition is given as

$$I_{sat} = h\nu/(\sigma\tau),$$

In the approximation that available Tm ions are efficiently and irreversibly pumped by excited Yb ions, the effective energy storage time corresponds to the Tm^{3+} $^3H_4$ value τ_{Tm} ~ 14 msec. [13] But since the absorption is occurring via the Yb ions, the cross section to use is $\sigma_{Yb} \sim 10^{-20}$ cm^2. The "effective capture cross section" is further enhanced by the factor $(N_{Yb}/N_{Tm}) \sim 350$. Therefore with respect to the $^3H_4$ level (first in the cascade), I_{sat}

$= (N_{Tm}/N_{Yb})(h\nu / \sigma_{Yb}\,\tau_{Tm}) \sim 4$ W/cm^2, while the value is ~30 W/cm^2 for the two-step process to the $^3F_4$ level, whose lifetime is ~2 msec [see Fig. 4(c).] Although we have not modeled the data, Fig. 3(c) clearly reveals that the two fluoride hosts exhibit efficiency saturation to a sub-linear intensity dependence at < 100 W/cm^2. This result is anticipated on the basis of the population of second electronic level of Tm reaching saturation near ~30 W/cm^2, as estimated above.

Conclusions

We have done upconversion-efficiency experiments in which a new approach was employed for pumping the phosphors. Use of a powerful, tunable, monochromatic source with a multimode fiber for pump-spot spatial formatting has removed some of the uncertainty regarding the excitation conditions. Such a technique was not possible in the early days of upconversion research. No convolution of illumination source and phosphor absorption spectra was required to calculate the absorbed intensity. Also, spatial inhomogeneity typical of early diode-laser output spots did not have to be considered.

Calibrated efficiency results were presented for several familiar phosphor powders and an easily-grown fluoride crystal—$Na_2Y_3F_{11}$:Yb,Er. Efficiencies ranged up to a few percent, but then saturated. This saturation could not be explored reliably with low-power laser sources, and our results call into question some of the extrapolations performed on data obtained with low-energy-density experiments. We have presented a simple model for the green upconversion efficiency vs pump intensity for Yb,Er - codoped samples; bottlenecking in the Er^{3+} $^4I_{13/2}$ level is postulated as the mechanism of saturation.

Several experiments could be done to extend this work. Detection of Er^{3+} $^4I_{13/2}$ 1500-nm radiation could be used to investigate the "bottleneck." Effects of sample morphology (crystal vs powder) could be performed on the $Na_2Y_3F_{11}$:Yb,Er system, which can be produced as a pure single crystal. Re-optimization of various phosphor recipes for use at high pump intensity may well give improved conversion efficiencies, especially in the blue. Short-pulse (microsecond) laser techniques, including pump-probe measurements, could be used to evaluate the various level populations in a bulk crystal, further elucidating the upconversion dynamics. Index-matching of powder samples would allow tests of diffusive-light-transport effects, that may actually be increasing the effective pump intensity in an experiment like ours. Much more ambitious modeling of upconversion efficiencies could be done if a better rate-constant data base were developed. The Yb,Tm system seems especially attractive in this regard on account of its perceived simplicity and absence of back-transfer effects.

Acknowledgements

We are especially grateful to Neil Yocom and Jim Kane for providing us with the upconversion phosphors from Sarnoff used for testing, and for sharing their insights regarding the effect of morphology, structure and dopants on upconversion efficiency. This work was performed under the auspices of the Office of Basic Energy Sciences, Department of Energy by the Lawrence Livermore National Laboratory under Contract W-

7405-ENG-48. Financial support was provided by the Gemfire Corporation, for which the LLNL authors are grateful. We wish also to acknowledge helpful discussions with Dr. Nigel Cockroft.

Figure Captions

Figure 1: (a) Experimental apparatus used to acquire the power conversion efficiency of the phosphors listed in Table I. Multimode - fiber - coupling provides a "flat-top" pump intensity profile. Calibration of the integrating - sphere/photodiode responsivity is accomplished with a series of low - power CW lasers at various wavelengths, and a sensitive power meter. (b) Detail of sample holder designed for use with powder samples. (c) Fiber - fed OMA setup for recording and calibrating phosphor emission spectra. The tungsten filament temperature is measured with a disappearing - filament pyrometer.

Figure 2: Spectrally - corrected emission spectra obtained for the phosphor materials, recorded at approximately the maximum Ti:sapphire laser pump power using the 200 μm fiber for delivery of the pump light. Spectra of the phosphors designated as green, red, and blue appear in frames A, B, and C, respectively.

Figure 3: Calibrated power conversion efficiencies obtained for the phosphor materials using a Ti:sapphire laser pump tuned to the wavelength corresponding to optimum efficiency (near 980 nm). The phosphors designated as green, red, and blue appear in parts A, B, and C, respectively. The efficiency scale (ordinate) includes normalization for the fraction of pump power absorbed in the phosphor, while the abscissa represents incident pump intensity at the fiber face, without a fraction-absorbed correction.

Figure 4: Energy level diagram depicting the pumping, radiation, cross - relaxation, and upconversion mechanisms relating to (a) the green-emitting Yb,Er phosphors, (b) the additional processes impacting the Yb,Er red phosphors, and (c) the Yb,Tm blue emitters. In each case, upconversion-pumping of the visible-luminescing species occurs by energy transfer from excited Yb^{3+} ions. Pumping and upconversion transitions are indicated with solid lines; squiggly lines denote radiation; zig-zags show radiationless decay; dashed lines represent cross - relaxation.

Figure 5: "Best" fit to the $Na_2Y_3F_{11}$:Yb,Er single - crystal power conversion effficiency data shown in Fig. 2(a), based on the use of eqs. (7) and (9), along with the definitions noted in Tables 2 and 3. The adjustable parameters were the Er upconversion constant γ_{upc}, and the cross-relaxation rate coefficients $\gamma^{X}_{3/2}$ (Er-Er) and $\gamma^{Y}_{3/2}$ (Er-Yb.) The rest of the input quantities are listed in Table 2.

References with titles

[1] N. Bloembergen, "Solid state infrared quantum counters," *Phys. Rev. Lett.* **2**, 84 - 85 (1959).

[2] TOKIN "IR catcher" (Tokin America, 155 Nicholson Lane, San Jose, California 95134;) LLNL internal characterization with X-ray diffraction.

[3] F. Heine, V. Ostroumov, E. Heumann, T. Jensen, G. Huber, and B. H. T. Chai, "CW Yb,Tm:YLF upconversion laser at 650 nm, 800 nm, and 1500 nm," OSA Proceedings on Advanced Solid-State Lasers **24**, 77 - 79 (1995); P. Xie and T. R. Gosnell, "Diode-pumped, CW, blue, green, orange, and red upconversion fiber lasers operating at room temperature," OSA Proceedings on Advanced Solid-State Lasers **24**, 101 - 105 (1995).

[4] E. Downing, L. Hesselink, J. Ralston, and R. Macfarlane, "A three-color, solid-state, three-dimensional display," *Science* **273**, 1185 - 1189 (1996).

[5] F. E. Auzel, "Materials and devices using double-pumped phosphors with energy transfer," *Proceedings of the IEEE* **61**, 758 - 788 (1973).

[6] T. Kano, H. Yamamoto, and Y. Otomo, "$NaLnF_4:Yb^{3+},Er^{3+}$ (Ln:Y,Gd,La): efficient green-emitting infrared-excited phosphors," *J. Electrochem. Soc.: Solid-State Sci.& Tech.* **119**, 1561 - 1564 (1972).

[7] H. Chou, P. Albers, A. Cassanho, and H. Jenssen, "CW Tunable Laser Emission of $Nd^{3+}:Na_{0.4}Y_{0.6}F_{2.2}$," Tunable Solid-State Lasers II :Proceedings of the OSA Topical Meeting (eds. A. B. Budgor, L. Esterowitz, L. G. DeShazer, Springer-Verlag Berlin Heidelberg, Germany, 1986) pg. 322.

[8] N. Menyuk, K. Dwight, and J. W. Pierce, "$NaYF_4$:Yb,Er—an efficient upconversion phosphor," *Appl. Phys. Lett.* **21**, 159 - 161 (1972) .

[9] P. N. Yocom, J. P. Wittke, and I. Ladany, "Rare-earth-doped oxysulfides for GaAs-pumped luminescent devices," *Metallurgical Transactions* **2**, 763 - 767 (1971).

[10] J. P. Wittke, I. Ladany, and P. N. Yocom, "Y_2O_3:Yb: Er — new red-emitting infrared-excited phosphor," *J. Appl. Phys.* **43**, 595 - 600 (1972).

[11] Y. Mita, H. Yamamoto, K. Katayanagi, and S. Shionoya, "Energy transfer processes in Er^{3+} - and Yb^{3+} - doped infrared upconversion materials," *J. Appl. Phys.* **78**, 1219 - 1223 (1995).

[12] J. E. Geusic, F. W. Ostermayer, H. M. Marcos, L. G. Van Uitert, and J. P. van der Ziel, "Efficiency of red, green, and blue infrared - to - visible conversion sources," *J. Appl. Phys.* **42**, 1958 - 1960 (1971).

[13] F. W. Ostermayer, "Preparation and properties of infrared - to - visible conversion phosphors," *Metallurgical Transactions* **2**, 747 - 755 (1971).

[14] R. A. Hewes and J. F. Sarver, "Infrared excitation processes for the visible luminescence of Er^{3+}, Ho^{3+}, and Tm^{3+}in Yb^{3+} - sensitized rare - earth trifluorides," *Phys. Rev.* **182**, 427 - 436 (1969).

[15] L. F. Johnson, H. J. Guggenheim, T. C. Rich, and F. W. Ostermayer, "Infrared - to - visible conversion by rare - earth ions in crystals," *J. Appl. Phys.* **43**, 1125 - 1137 (1972).

[16] J. D. Kingsley, G. E. Fenner, and S. V. Galginaitis, "Kinetics and efficiency of infrared-to-visible conversion in LaF_3:Yb,Er," *Appl. Phys. Lett.* **15**, 115 - 117 (1969).

[17] E. Okamoto, H. Masui, K. Muto, and K. Awazu, "Nonresonant energy transfer from Er^{3+} to Yb^{3+} in LaF_3," *J. Appl. Phys.* **43**, 2122 - 2123 (1972).

[18] M. A. Chamarro and R. Cases, "Infrared to visible upconversion of Er^{3+} in Yb^{3+} doped fluorohafnate glasses," *J. Luminesc.* **46**, 59 - 65 (1990).

[19] F. Auzel, D. Pecile, and D. Morin, "Rare earth doped vitroceramics: new, efficient, blue and green emitting materials for infrared upconversion," *J. Electrochem. Soc.: Solid-StateSci.& Tech.* **122**, 101 - 107 (1975).

[20] J. P. Wittke, I. Ladany, and P. N. Yocom, "Properties of a blue-emitting IR pumped YF_3:Yb,Tm diode," *Proc. IEEE (Lett.)* **58**, 1283-1285 (1970).

[21] Y. Wang and J. Ohwaki, "High-efficiency infrared-to-visible conversion of Er^{3+} in $BaCl_2$," *J. Appl. Phys.* **74**, 1272 - 1278 (1993).

[22] S. L. Jacques, "Role of tissue optics and pulse duration on tissue effects during high-power laser irradiation," *Appl. Opt.* **32**, 2447 - 2454 (1993).

[23] A. Bril, J. L. Sommerdijk, and A. W. de Jager, "On the efficiency of Yb^{3+} - Er^{3+} activated up-conversion phosphors," *J. Electrochem. Soc.: Solid-State Sci.& Tech.* **122**, 660 - 663 (1974).

[24] F. Auzel and D. Pecile, "Comparison and efficiency of materials for summation of photons assisted by energy transfer," *J. Luminesc.* **8**, 32 - 43 (1973).

[25] A. Kermaoui, G. Özen, PH. Goldner, J. P. Denis, and F. Pellé, "Infrared to blue upconversion fluorescence in heavy metal fluoride glass codoped with Tm^{3+} and Yb^{3+} ions," *J. Phys. Chem. Solids* **55**, 677 - 682 (1994).

[26] G. Özen, J. P. Denis, Xu Wu, F. Pellé, and B. Blanzat, "Upconversion luminescence of Tm^{3+} in Yb^{3+} - doped fluorophosphate glasses under 683 nm excitation," *J. Non-Crystalline Solids* **176**, 147 - 156 (1994).

[27] D. C. Yeh, W. A. Sibley, and M. J. Suscavage, "Efficient frequency upconversion of Tm^{3+} ions in Yb^{3+} doped barium - thorium - fluoride glass," *J. Appl. Phys.* **63**, 4644 - 4650 (1988).

[28] T. C. Rich and D. A. Pinnow, "Exploring the ultimate efficiency in infrared-to-visible converting phosphors activated with Er and sensitized with Yb," *J. Appl. Phys.* **43**, 2357 - 2365 (1972).

[29] A. A. Kaminskii, Crystalline Lasers: Physical Processes and Operating Schemes (CRC Press, Boca Raton, Florida, 1996), pg. 275.

[30] J. Wright, "Up - conversion and excited state energy transfer in rare - earth doped materials," ch. 4 in Radiationless processes in molecules and condensed phases, F. K. Fong, ed., Top. Appl. Phys. **15** (Springer, NY, 1976) 239 - 295.

[31] Y. Mita, "Luminescence processes in Yb^{3+} - sensitized rare - earth phosphors," *J. Appl. Phys.* **43**, 1772 - 1778 (1972).

[32] J. D. Kingsley, "Analysis of energy transfer and infrared-to-visible conversion in LaF_3:Yb,Er,"*J. Appl. Phys.* **41**, 175 - 182 (1970).

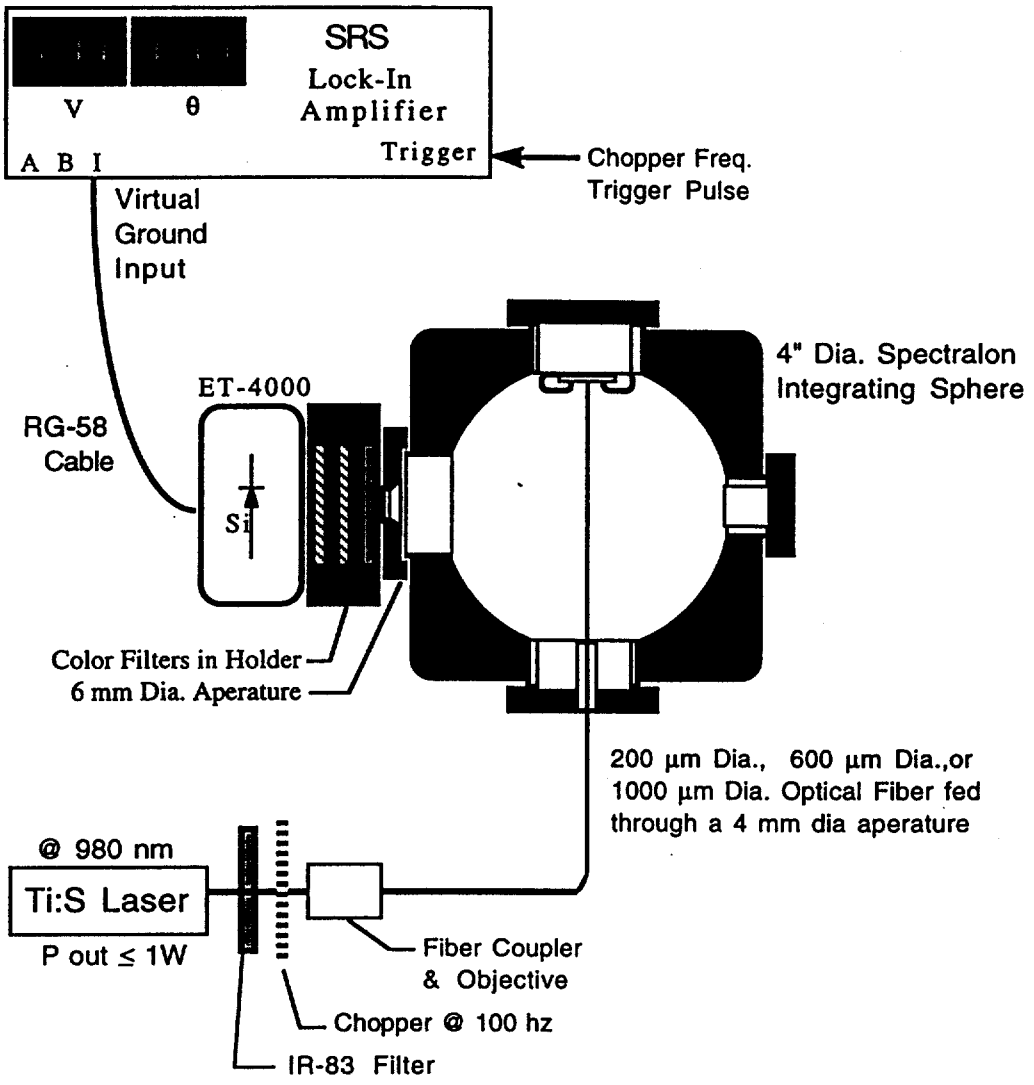
SRS
Lock-In
Amplifier
V
θ
A B I
Trigger
Chopper Freq.
Trigger Pulse
Virtual
Ground
Input
RG-58
Cable
ET-4000
Si
4" Dia. Spectralon
Integrating Sphere
Color Filters in Holder
6 mm Dia. Aperature
200 µm Dia., 600 µm Dia.,or
1000 µm Dia. Optical Fiber fed
through a 4 mm dia aperature
@ 980 nm
Ti:S Laser
P out ≤ 1W
Fiber Coupler
& Objective
Chopper @ 100 hz
IR-83 Filter

Fig 1(a)

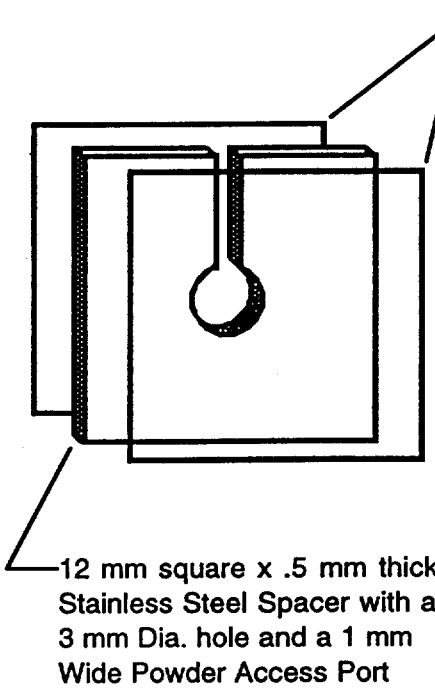

Powder Sample Cell

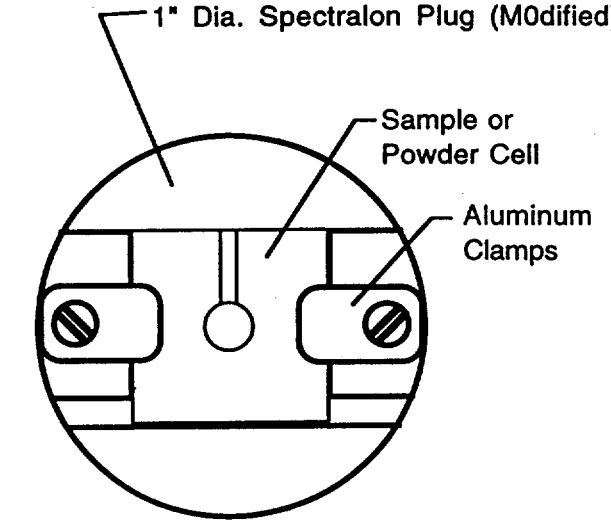

Sample Cell Mount

Fig 1(b) / inset

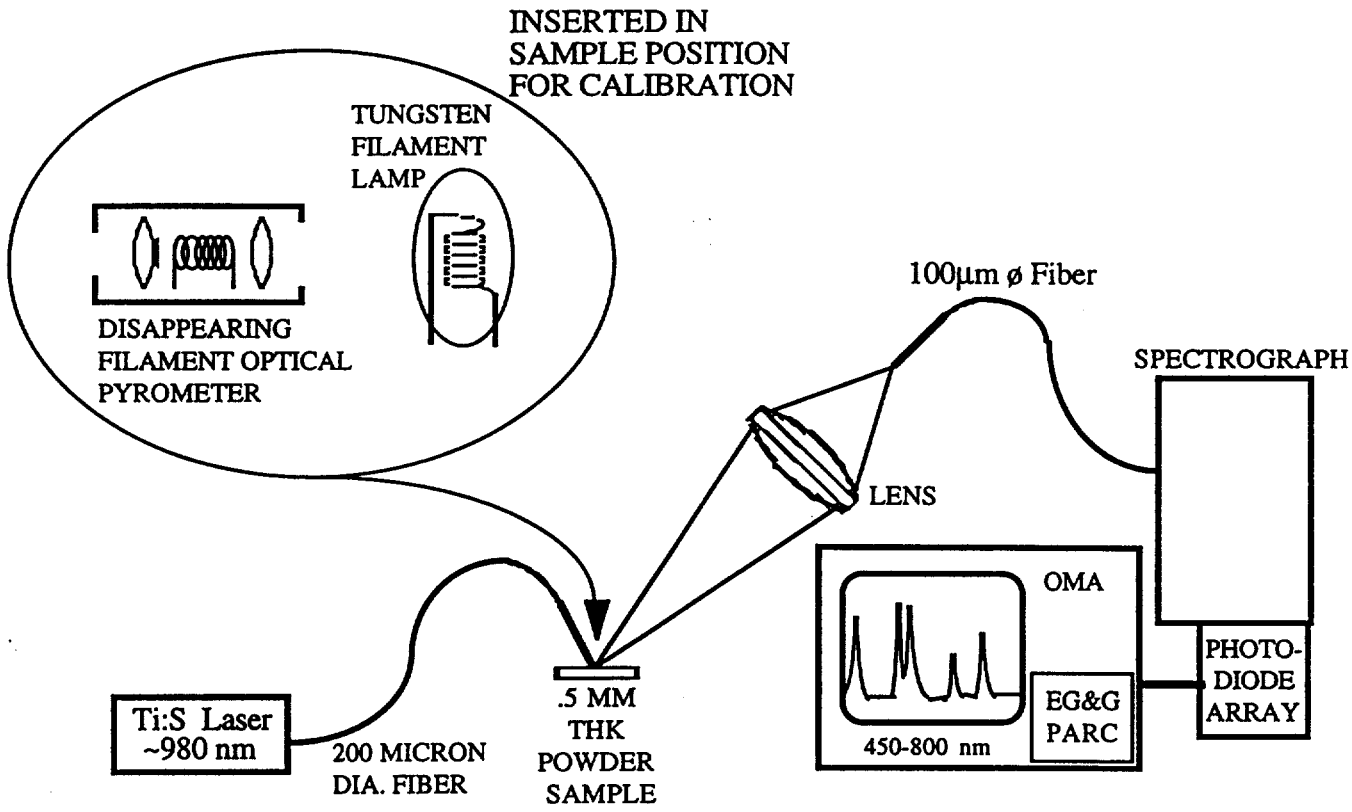
INSERTED IN
SAMPLE POSITION
FOR CALIBRATION
TUNGSTEN
FILAMENT
LAMP
DISAPPEARING
FILAMENT OPTICAL
PYROMETER
100µm ø Fiber
SPECTROGRAPH
LENS
OMA
PHOTO-
DIODE
ARRAY
EG&G
PARC
450-800 nm
Ti:S Laser
~980 nm
200 MICRON
DIA. FIBER
.5 MM
THK
POWDER
SAMPLE

Fig. 1(c)

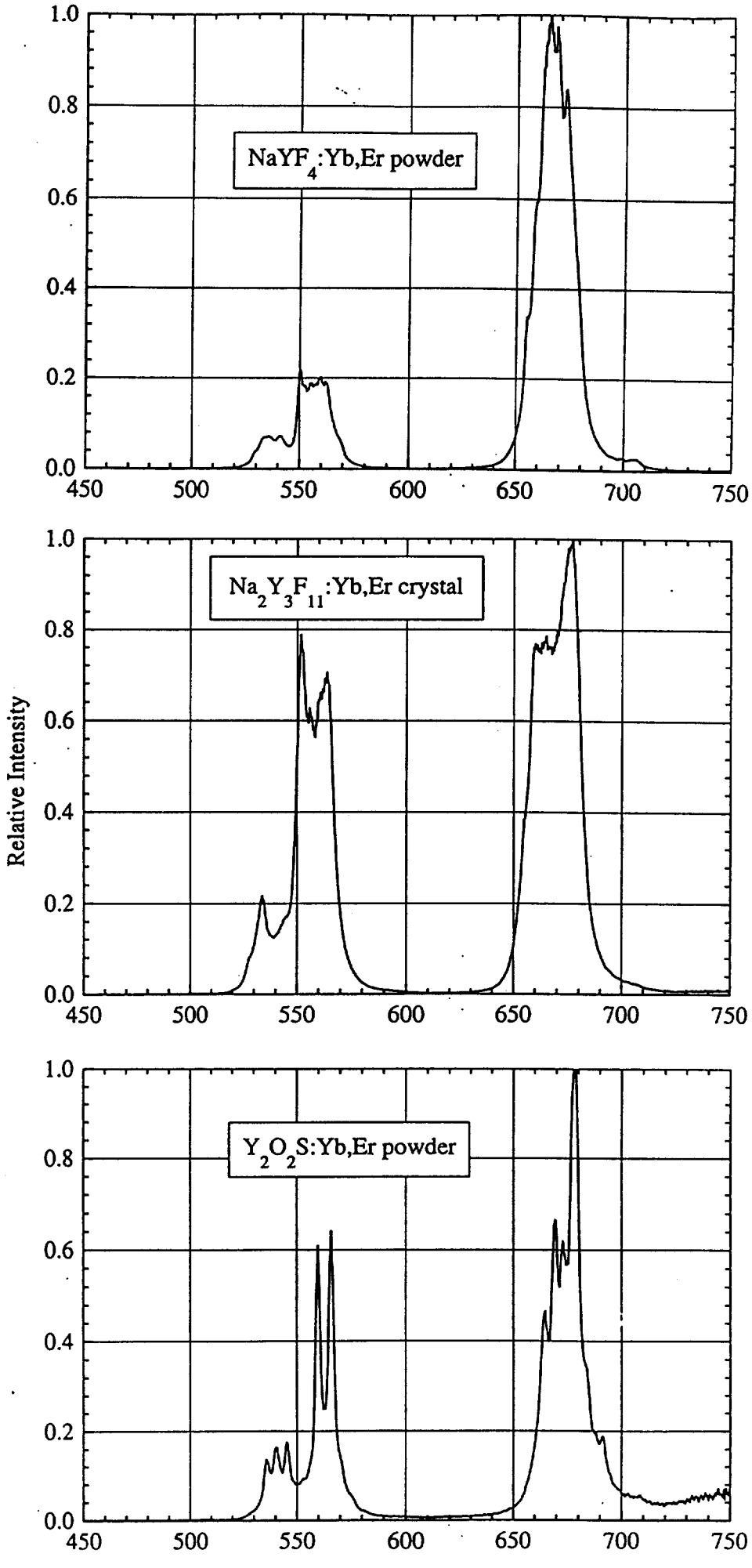
NaYF4:Yb,Er powder
Na2Y3F11:Yb,Er crystal
Y2O2S:Yb,Er powder
Relative Intensity
Wavelength (nm)
1.0
0.8
0.6
0.4
0.2
0.0
450
500
550
600
650
700
750

Fig 2 (a)

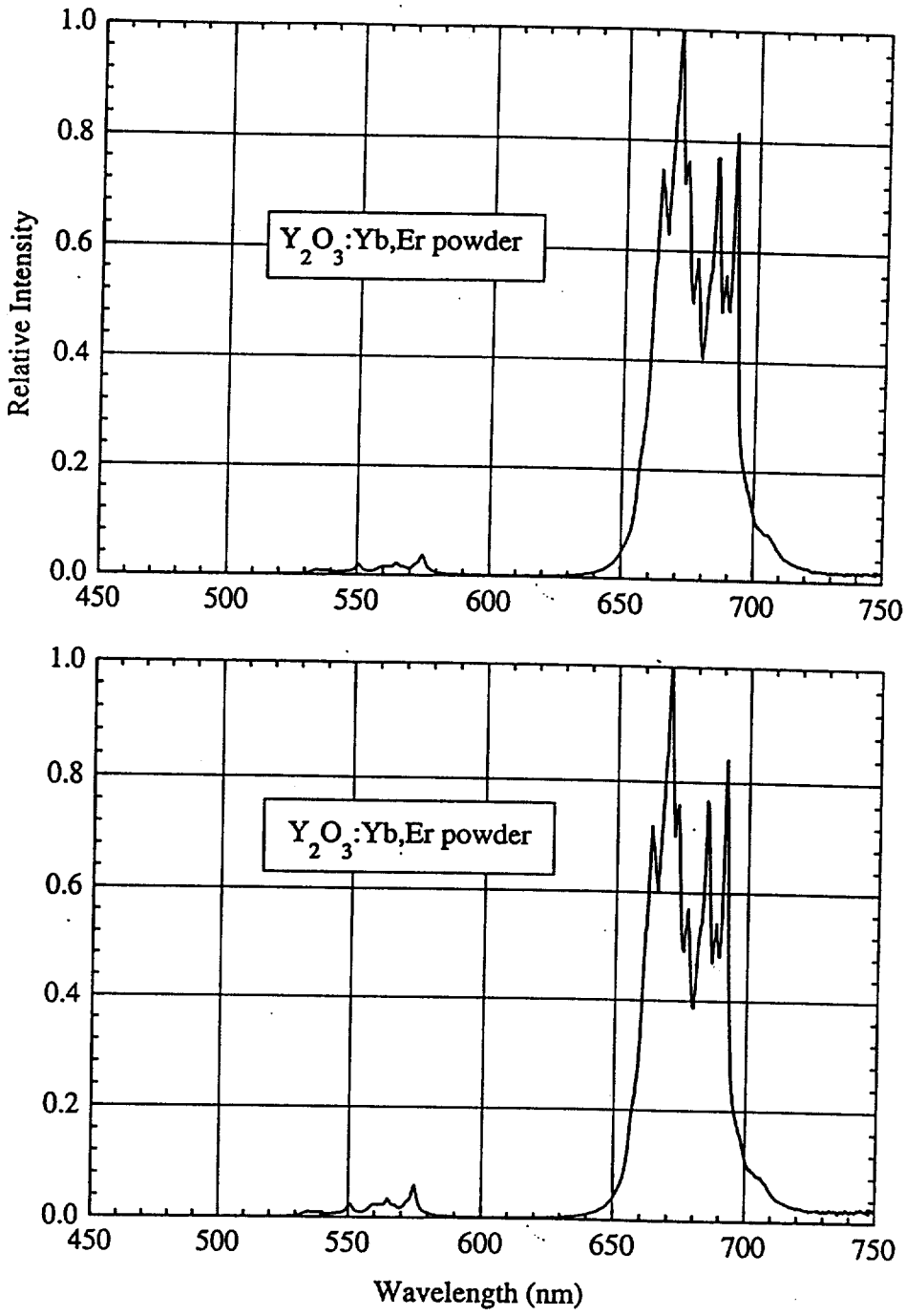
1.0
0.8
0.6
0.4
0.2
0.0
Relative Intensity
Y_2O_3:Yb,Er powder
450
500
550
600
650
700
750
Y_2O_3:Yb,Er powder
Wavelength (nm)

Fig 2(b)

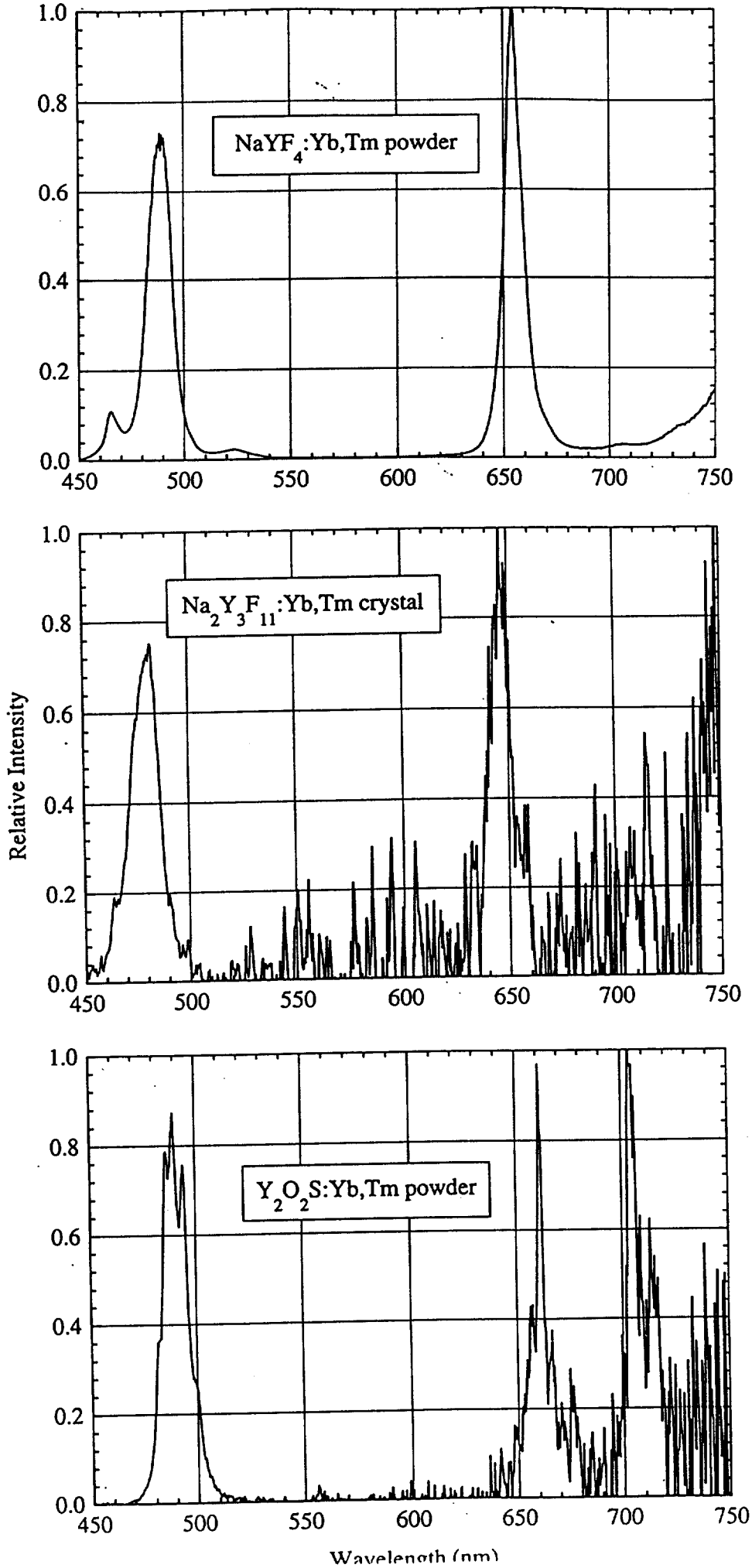
NaYF4:Yb,Tm powder
Na2Y3F11:Yb,Tm crystal
Y2O2S:Yb,Tm powder
Relative Intensity
Wavelength (nm)
1.0
0.8
0.6
0.4
0.2
0.0
450
500
550
600
650
700
750

Fig 2(c)

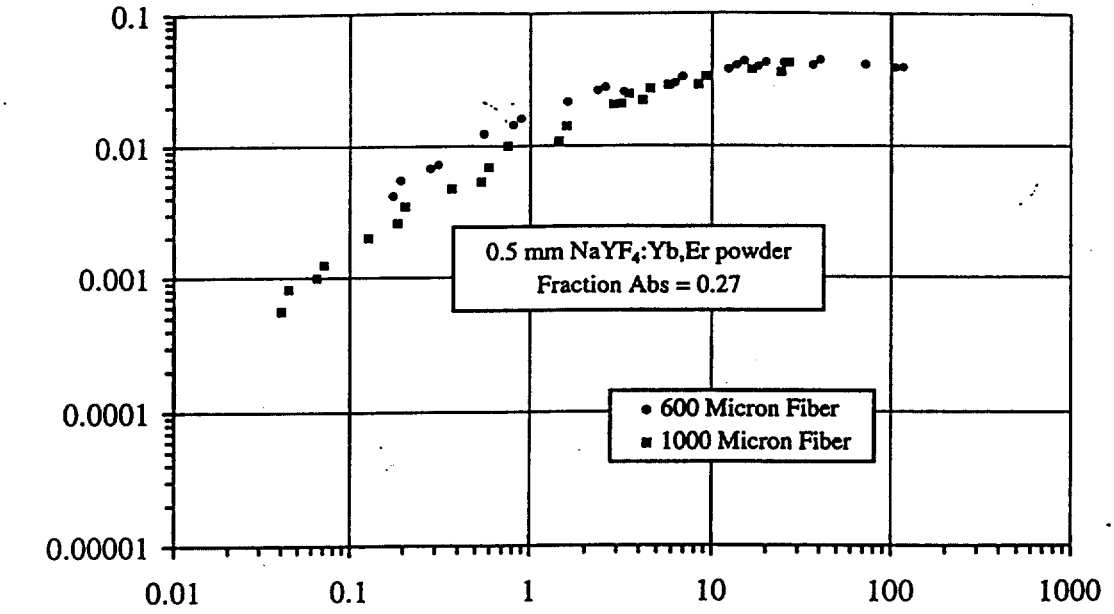

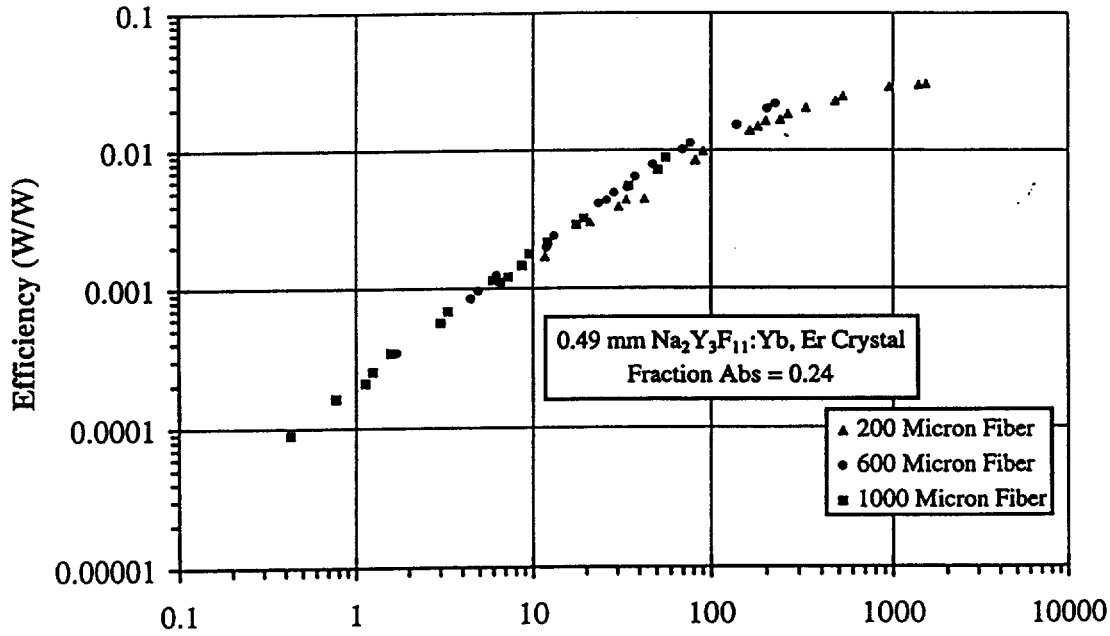

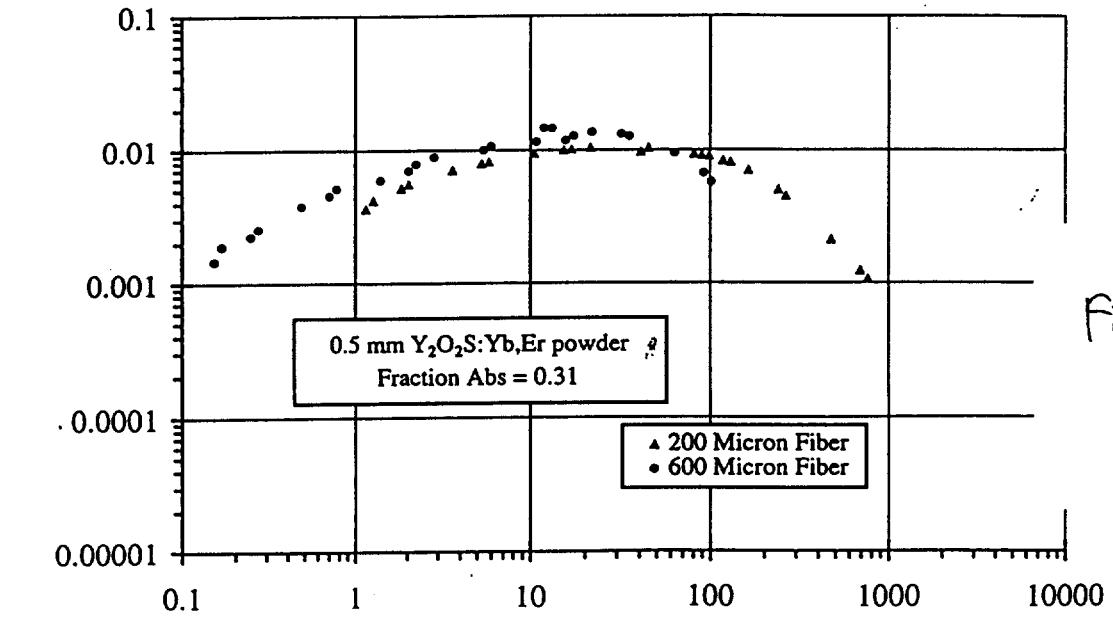

Efficiency (W/W)

Pump Intensity (W/cm^2)

Fig 3(a)

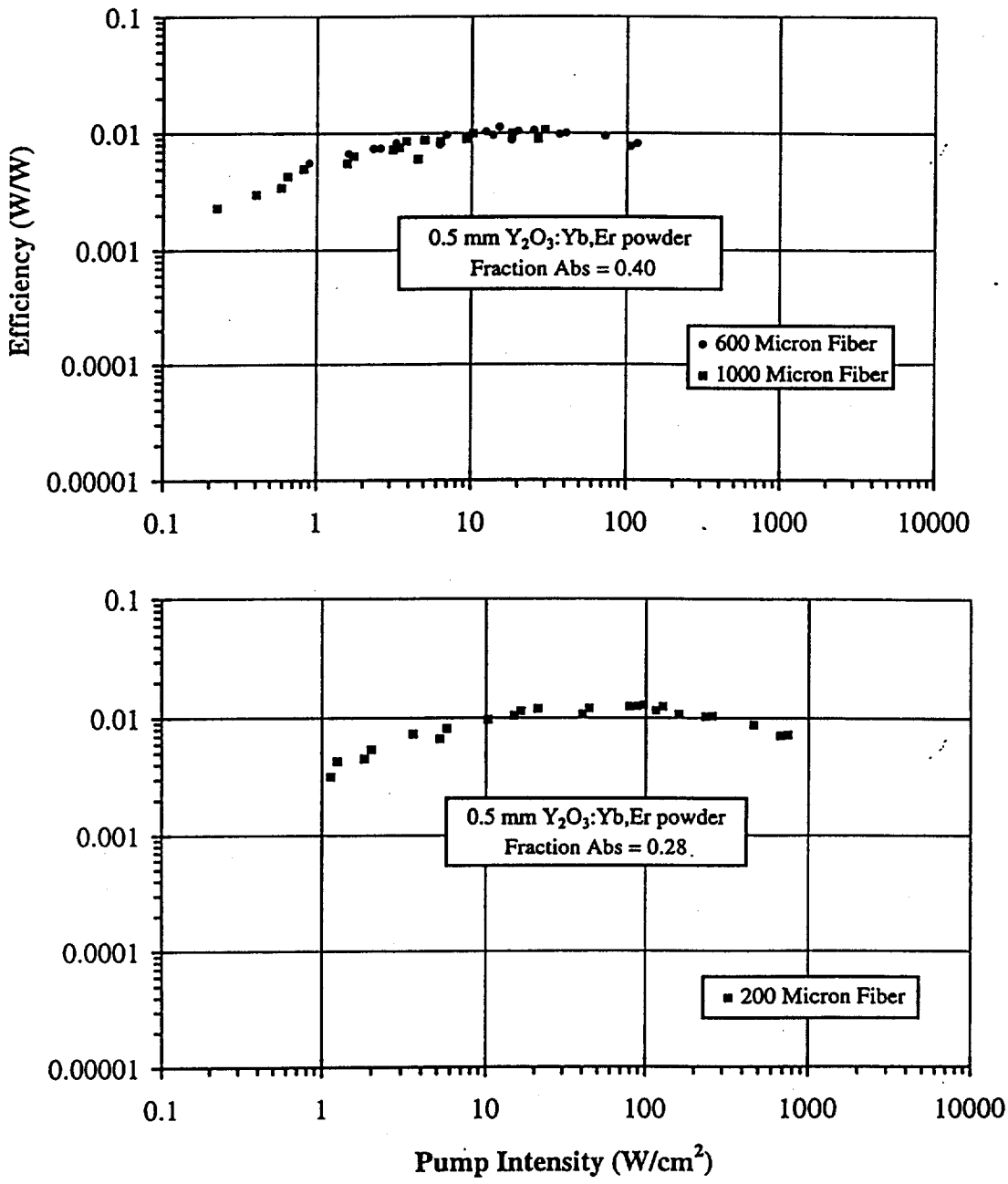
Efficiency (W/W)
0.1
0.01
0.001
0.0001
0.00001
0.1
1
10
100
1000
10000
0.5 mm Y_2O_3:Yb,Er powder
Fraction Abs = 0.40
• 600 Micron Fiber
▪ 1000 Micron Fiber
0.5 mm Y_2O_3:Yb,Er powder
Fraction Abs = 0.28
▪ 200 Micron Fiber
Pump Intensity (W/cm^2)

Fig 3(b)

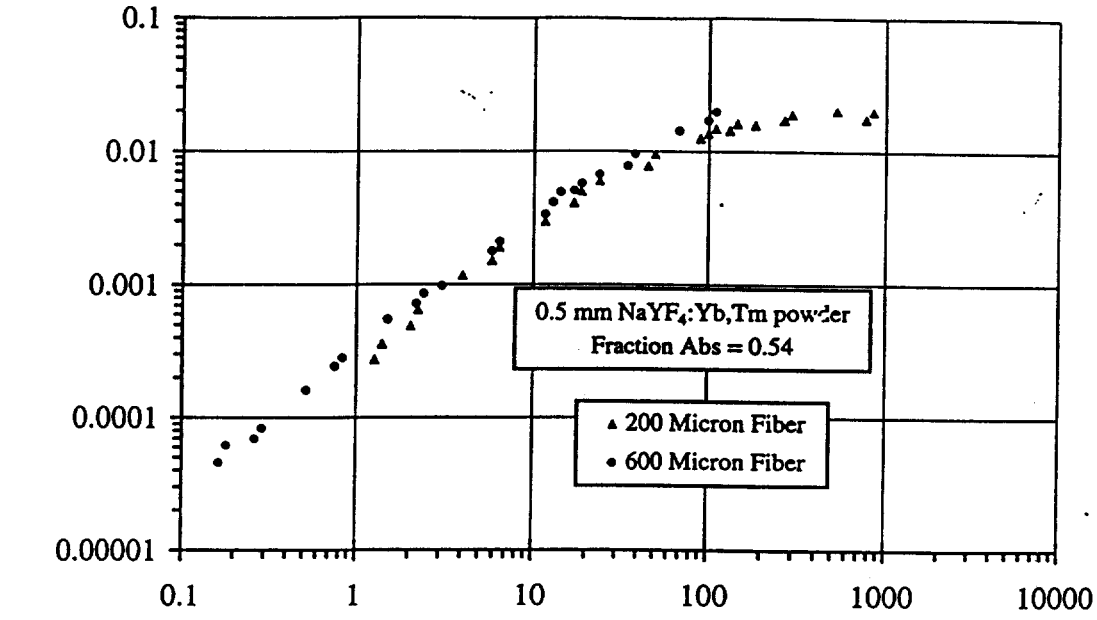
0.1
0.01
0.001
0.0001
0.00001
0.1
1
10
100
1000
10000
0.5 mm NaYF4:Yb,Tm powder
Fraction Abs = 0.54
200 Micron Fiber
600 Micron Fiber

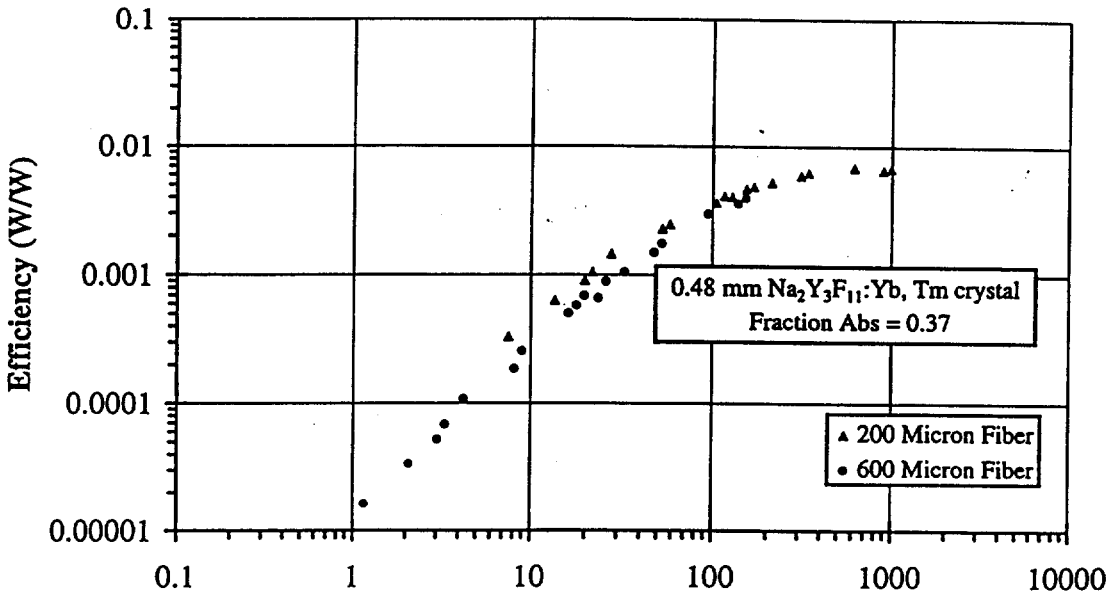
Efficiency (W/W)
0.1
0.01
0.001
0.0001
0.00001
0.1
1
10
100
1000
10000
0.48 mm Na2Y3F11:Yb, Tm crystal
Fraction Abs = 0.37
200 Micron Fiber
600 Micron Fiber

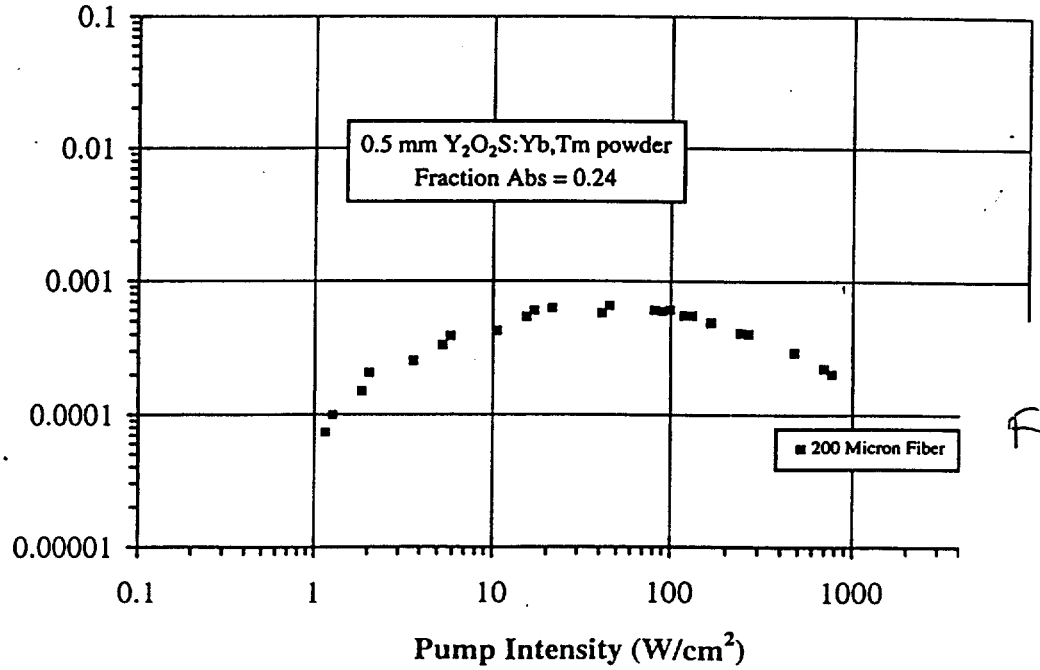
0.1
0.01
0.001
0.0001
0.00001
0.1
1
10
100
1000
0.5 mm Y2O2S:Yb,Tm powder
Fraction Abs = 0.24
200 Micron Fiber
Pump Intensity (W/cm2)

Fig 3(b)

Figure 4

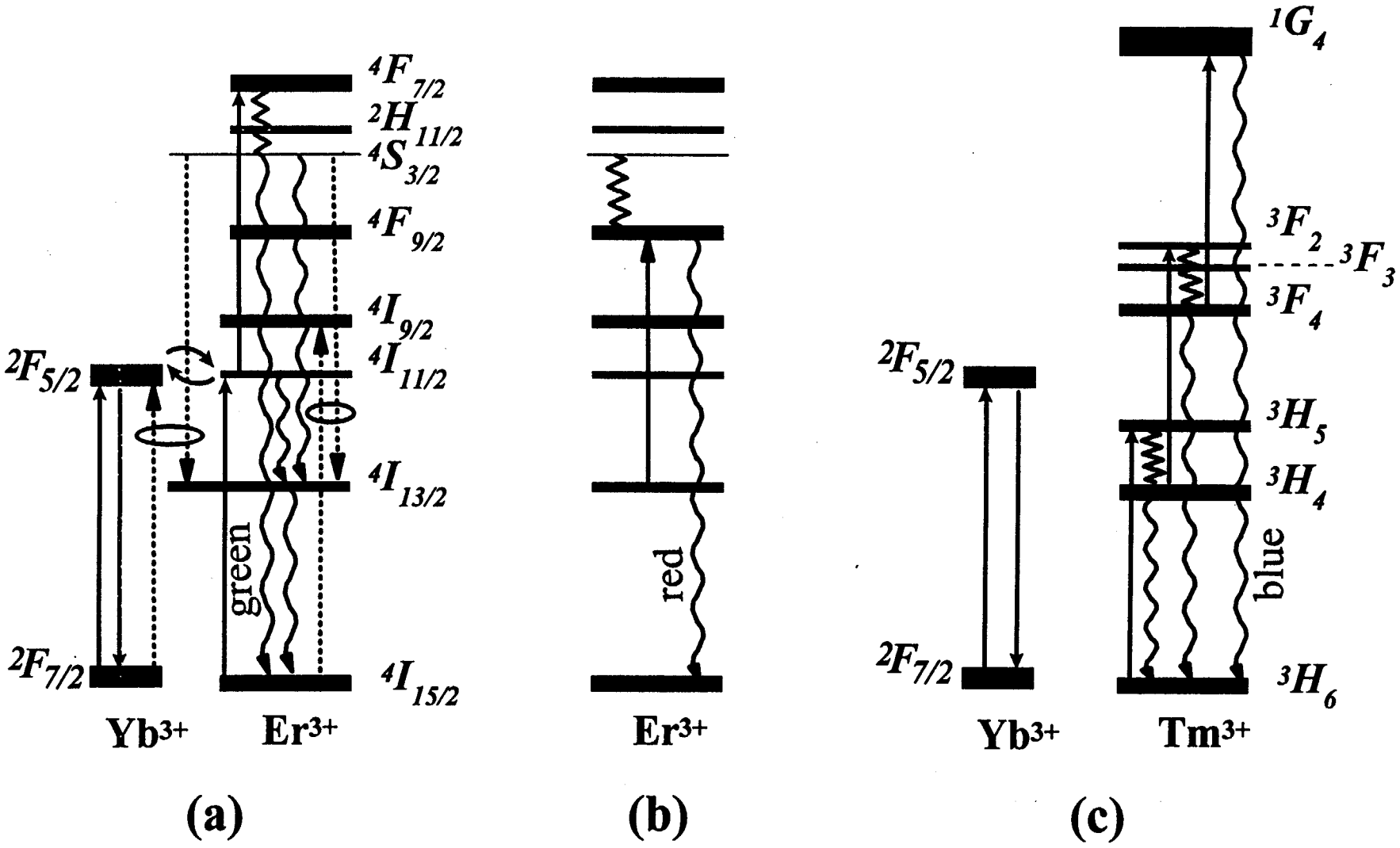
$^4F_{7/2}$
$^2H_{11/2}$
$^4S_{3/2}$
$^4F_{9/2}$
$^4I_{9/2}$
$^4I_{11/2}$
$^4I_{13/2}$
$^4I_{15/2}$
$^2F_{5/2}$
$^2F_{7/2}$
green
Yb3+
Er3+
(a)
red
Er3+
(b)
$^1G_4$
$^3F_2$
$^3F_3$
$^3F_4$
$^3H_5$
$^3H_4$
$^3H_6$
blue
$^2F_{5/2}$
$^2F_{7/2}$
Yb3+
Tm3+
(c)

Green upconversion efficiency vs pump intensity

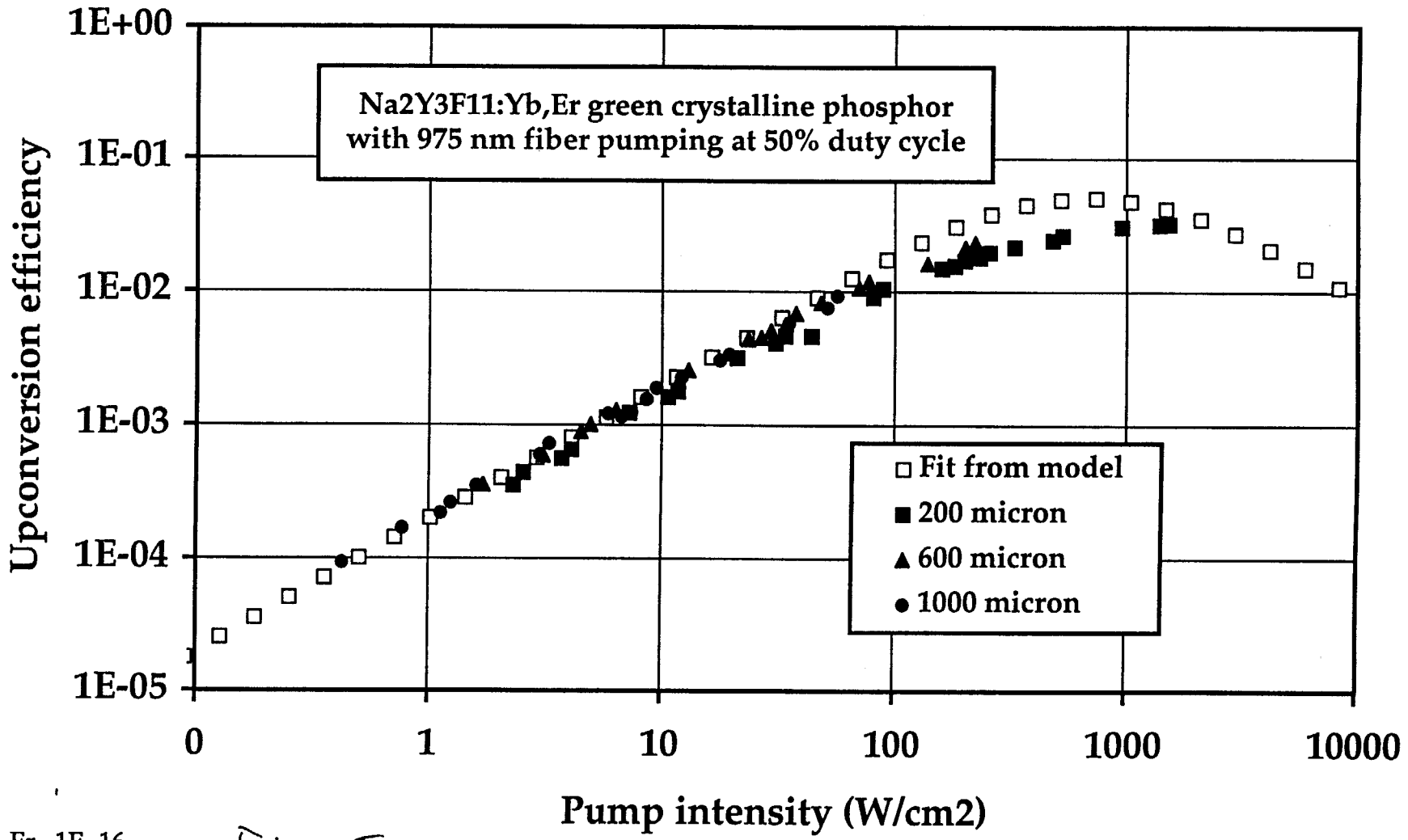

Er - Er 1E -16
Er - Yb 5E-18
upc 1E-17
tau 94 usec

Fig - 5
(new)

Technical Information Department • **Lawrence Livermore National Laboratory**
University of California • Livermore, California 94551